Mechanisms of Pathogenicity of Hypertrophic Cardiomyopathy-Associated Troponin T *(TNNT2)* Variant R278C$^{+/-}$ During Development

Sanam Shafaattalab[1,2,α], Alison Y Li[1,2,α], Farah Jayousi[1,2,α], Yasaman Maaref[1,2,α], Homa Hamledari[1,2], Dina Hosseini Baygi[1,2], Tiffany Barszczewski[1,2], Marvin Gunawan[1,2], Balwinder Ruprai[1,2], Shayan Jannati[1,3], Raghu Nagalingam[1,2], Austin M Cool[4], Paulina Langa[5], R John Solaro[5], Shubhayan Sanatani[1], Christopher Toepfer[6], Steffen Lindert[3], Philipp Lange[7,8], Glen F Tibbits[1,2,9,10*]

[α]These authors contributed equally to this study

1. Cellular and Regenerative Medicine Centre, BC Children's Hospital Research Institute, Vancouver, BC, V5Z 4H4, Canada
2. Biomedical Physiology and Kinesiology, Simon Fraser University, Burnaby, BC, V5A 1S6, Canada
3. Mechanical Engineering, University of British Columbia
4. Department of Chemistry and Biochemistry, Ohio State University, Columbus, OH, USA
5. Department of Physiology and Biophysics, College of Medicine, University of Illinois at Chicago, , Chicago, IL, 60612, USA
6. University of Oxford, Oxford, UK
7. Pathology and Laboratory Medicine, University of British Columbia, Vancouver, BC
8. Michael Cuccione Childhood Cancer Research Program, BC Children's Hospital Research Institute, Vancouver, BC
9. Molecular Biology and Biochemistry, Simon Fraser University, Burnaby, BC, V5A 1S6, Canada
10. School of Biomedical Engineering, University of British Columbia, Vancouver, BC, Canada

*Correspondence:
Glen F Tibbits, PhD
Cellular and Regenerative Medicine Centre
BC Children's Hospital Research Institute
938 West 28th Avenue
Vancouver, BC, V5Z 4H4
Canada

tibbits@sfu.ca

Abstract

Hypertrophic cardiomyopathy (HCM) is one of the most common heritable cardiovascular diseases and variants of *TNNT2* (cardiac troponin T) are linked to increased risk of sudden cardiac arrest despite causing limited hypertrophy. In this study, a *TNNT2* variant, R278C$^{+/-}$, was generated in both human cardiac recombinant/reconstituted thin filaments (hcRTF) and human-induced pluripotent stem cells (hiPSCs) to investigate the mechanisms by which the R278C$^{+/-}$ variant affects cardiomyocytes at the proteomic and functional levels. The results of proteomics analysis showed a significant upregulation of markers of cardiac hypertrophy and cardiac remodeling in R278C$^{+/-}$ vs. the isogenic control. Functional measurements showed that R278C$^{+/-}$ variant increases the myofilament sensitivity to Ca^{2+}, increases the kinetics of contraction, and causes arrhythmia at frequencies >75 bpm. This study uniquely shows the profound impact of the *TNNT2* R278C$^{+/-}$ variant on the cardiomyocyte proteomic profile, cardiac electrical and contractile function in the early stages of cardiac development.

Introduction

Hypertrophic cardiomyopathy (HCM) is one of the most common inherited heart diseases and is associated with >1500 variants located in ~20 genes with the majority encoding for sarcomeric and Z-disks proteins[1,2]. HCM is an autosomal dominant inherited disorder that is characterized by asymmetrical left ventricular hypertrophy, enhanced contractility, impaired relaxation, and myofibrillar disarray, which clinically can manifest sudden cardiac arrest (SCA) [3,4]. The most common variants are in sarcomeric genes including cardiac myosin-binding protein C (*MYBPC3*), β-myosin heavy chain (*MYH7*) and cardiac troponin T (*TNNT2).* Despite being the most known cause of sudden cardiac arrest in youth, the mechanisms by which HCM can result in SCA are not well understood and targeted therapeutics are still very limited. The latter is due primarily to the serious limitations of research studies using animal models and samples obtained from diseased patients[4]. It is generally believed that the various genetic variants associated with HCM result in defects in the biophysical dynamics of Ca^{2+} handling and contractility[4–7], which signal significant alterations in the transcriptome, proteome, and function. The HCM-linked *TNNT2* variants are of clinical interest because there is evidence that they are less likely to be associated with cardiac hypertrophy and therefore less likely to be diagnosed by echocardiography[8].

Previous investigations have mostly relied on animal models, predominantly rodents, to investigate disease pathogenesis and therapeutic options in cardiomyopathies and associated complications such as SCA. However, the promising outcomes and clinical translation have been limited due to substantial physiological and pharmacological differences between humans and rodents[9].

Recent studies have used hiPSC-CMs based disease models to investigate the underlying causes and consequences of HCM-linked variants[9]. Schuldt et al[10] observed a dose-dependent relationship between *TNNT2* R278C$^{+/-}$ protein expression dose and myofilament function in the detergent-extracted cardiomyocytes from the interventricular septum of *TNNT2* R278C$^{+/-}$ patients using troponin exchange experiments. The *TNNT2* R278C$^{+/-}$ variant showed increased Ca^{2+} sensitivity at low doses and a significant increase at intermediate doses. Although a high dose significantly decreased Ca^{2+} sensitivity[10], others observed no tendency towards increased myofilament Ca^{2+} sensitivity or arrhythmogenicity in transgenic mice overexpressing the R278C$^{+/-}$ *TNNT2*[11,12]. We have previously shown that human HCM-associated *TNNT2* variants can enhance myofilament Ca^{2+} sensitivity, alter the action potential and modify contractile kinetics in human iPSC-CMs[13].

Due to the paucity of studies on the *TNNT2* R278C$^{+/-}$ variant, we sought to address this area in more detail using human iPSC-CMs and human cardiac recombinant/reconstituted thin filaments (hcRTF) for the following reasons: 1) there is compelling clinical evidence that the R278C$^{+/-}$ variant can trigger arrhythmias and sudden cardiac arrest[10,14,15]; 2) the arginine at residue 278 is highly conserved over four million years of evolution (**Figure S1**); and 3) molecular mechanics potential energy minimization calculations strongly suggest the R278C$^{+/-}$ variant alters the interaction of *TNNT2* with tropomyosin (Tm) (**Figure 1**).

In this study, both human cardiac recombinant/reconstituted thin filaments (hcRTF) and human iPSCs were used to determine the changes in cardiac function and the proteome. Whereas the in vitro motility assay can provide details of the Ca^{2+} kinetics and assessment of actin-myosin interaction, it cannot represent the whole sarcomere as sarcomere length is not a controllable variable. While one of the limitations of using hiPSC-CMs is their relative immaturity, we have used hiPSC-CMs to better understand the consequences of HCM-associated variants at early stages of development. The CRISPR/Cas9 genome-editing was used to generate heterozygous R278C$^{+/-}$ *TNNT2* hiPSC-CMs. The proteomic analysis was conducted in hiPSC-CMs using mass spectrometry (MS). Since increased contractility and impaired relaxation are hallmarks of cardiomyocytes harboring HCM causing genetic variants, measurement of these parameters is essential to understanding this disease. Therefore, a MATLAB based algorithm SarcTrack[16] was used to assess sarcomere shortening, contraction, and relaxation kinetics of 2D monolayers of hiPSC-CMs. Since mavacamten has been approved by the FDA to treat obstructive HCM, the response of different HCM causing genetic variants of both the thick and thin filaments, it is worthy of further investigation. Mavacamten, an allosteric myosin ATPase inhibitor, reduces the number of myosin heads available to interact with actin by promoting the super relaxed state (SRX) state and is thought to improve diastolic dysfunction in HCM patients[17]. Since HCM has a highly dynamic clinical evolvement, determining the effect of mavacamten on HCM causing *TNNT2* variants is of prime importance. Lastly, optical mapping was used to investigate the propensity for arrhythmias induced by the R278C$^{+/-}$ variant in hiPSC-CMs. In this study, we attempt to fill the gap of this *TNNT2* R278C$^{+/-}$ hiPSC-CMs model recapitulates key cellular features of HCM linked variants which provide us with necessary insight into the physiology and pathophysiology of the HCM.

This unique approach in studying the early impact of the *TNNT2* HCM-related variant R278C$^{+/-}$ on cardiomyocyte proteomic profile and function has generated a magnitude of novel data that could be very impactful on understanding this disease.

Methods

Computational Modelling and Potential Energy Minimization

To obtain a model of the thin filament complex, the PDB structures 6KN7 (Ca^{2+} free) and 6KN8 (Ca^{2+} bound) were used[18]. Each of these structures contains two troponin complexes, with cardiac troponin T (cTnT) being designated as chains "a" and "T", respectively. Both cTnT chains have contacting actin and tropomyosin subunits, in which chain a is close to chains G (actin) and P (tropomyosin) and chain T is close to chains F (actin) and W (tropomyosin). None of the four TnT structures (6KN7a, 6KN7T, 6KN8a, and 6KN8T) contains residue R278, with each cTnT structure being truncated at residue Q272.

Rosetta was utilized to build residues 273-281, using the sequence: KVSKTRGKA. Each of the four TnT chains (6KN7a, 6KN7T, 6KN8a, and 6KN8T) was removed from the thin filament complex and 1,000 models were built of the existing structure plus residues 273-281 using the loop modeling application of Rosetta[19,20]. This was done twice, the first designated all the residues to be built as a helical structure, the second designated all the residues to be built as an unstructured loop. In both cases, Rosetta built residues 273-281 as a helical structure. The top scoring model was then placed into its original PDB structure to generate a thin filament model that contained the cTnT R278 residue.

Four more models were then created by introducing the $R278C^{+/-}$ variant into the models produced by Rosetta. Each of the eight models of the thin filament complex were then solvated with explicit TIP3W water molecules and NaCl counterions were added to neutralize the entire system and establish a final salt concentration of 150mM. The resulting models were subjected to two sequential 10,000 potential energy minimization steps using Nanoscale Molecular Dynamics (NAMD)22 in the Charmm36 force field. This was done to optimize the positions of the solvent molecules around the protein and to subsequently relax the positions of residue side chain atoms. To analyze the models, residues that were within a certain cutoff of the gamma carbon (CG) atom of the R278 residue of the native structure and of the gamma sulfur (SG) atom of the C278 residue in the mutated models, were recorded.

Generation of human cardiac reconstituted thin filaments (hcRTF)

Recombinant human adult troponin subunits were used to generate the cardiac troponin complexes (cTn). Recombinant human α-Tm produced in *E. coli* does not undergo an acetylation process[21] and the unacetylated initial Met binds actin poorly and does not polymerize. In this study, the recombinant αTm included an MAS peptide (Met-Ala-Ser) added to the N-terminus to mimic the acetylation process and ensure actin binding[21]. The purification of each protein was verified by gel electrophoresis. Reconstituted thin filaments were then generated by mixing each cTn complex with human αMAS *TPM1* as well as native actin extracted from rabbit skeletal muscle which has a 99.2% sequence identity with human cardiac actin[22]. The stopped flow assay used for testing the functional validity of the hcRTF in this study has been described by Davis et al. 2007[23].

Determination of hcRTF Ca^{2+} kinetics

The Ca^{2+} off rate constants ($k_{off\ (Ca^{2+})}$) from each hcRTF were characterized using a Chirascan stopped-flow apparatus (Applied Photophysics, Surrey, UK) with a dead time of 1.1 ms at 15.0 ± 0.1°C. 2-(4'-(iodoacetoamido)anilino) naphthalene-6-sulfonic acid (IAANS) fluorophore was attached to residue C53 of TnC, was excited at 300 nm and monitored through a 510 nm broad band-pass interference filter (Semrock, Rochester, NY) as described by Davis et al[23]. Each trace was obtained as the solution containing hcRTF saturated with 200 µM $CaCl_2$ was rapidly mixed with 10 mM EGTA solution in the stopped-flow buffer containing (in mM): 10 MOPS, 150 KCl, 3 $MgCl_2$, 1 DTT, pH 7.0. Each $k_{off(Ca)}$ value represents an average of at least five traces fit with a single exponential equation and repeated more than 15 times. Two means were considered to be significantly different when $p \leq 0.05$.

All steady-state fluorescence measurements were performed using a Cary Eclipse fluorescence spectrophotometer (Agilent, country/state) at 15 ± 0.1°C as described[22]. In brief, the IAANS fluorophore was excited at 330 nm and monitored at the peak of the emission at 450 nm. Microliter amounts of $CaCl_2$ were added to 2 mL of each labeled hcRTF in a titration buffer containing (in mM): 200 MOPS, 150 KCl, 3 $MgCl_2$, and 1 DTT at pH 7.0. At least five to eight datasets were collected for each construct and the data were fit with a sigmoidal fit (based on the Hill equation) in Origin 8.5 (Microcal Software, Northampton, MA). The Ca^{2+} sensitivity for each hcRTF was represented by the dissociation constant K_d (± SEM) defined as the Ca^{2+} concentration at the half-maximal fluorescence change. Two means were significantly different when $p \leq 0.05$.

Human iPSC maintenance and cardiomyocyte differentiation

Human iPSC lines were obtained from the Wicell Research Institute (iPS IMR90-1) (https://www.wicell.org/) and the Allen Institute (https://alleninstitute.org/). Differentiation of hiPSCs to ventricular cardiomyocytes (hiPSC-CMs) employed a protocol published previously[22]. In brief, hiPSCs were maintained on a Corning Matrigel (0.5 mg/ 6-well plate, dissolved in DMEM/F-12 medium) cultured in mTeSR1 medium (StemCell Technologies, Vancouver, BC). Cells were passaged every 4 days using Versene solution (ThermoFisher, Waltham, MA) and were then seeded on a 6-well Matrigel-coated plate at a density of 100,000 cells cm^{-2} in mTeSR1 medium. The medium was changed daily, and after 3 to 4 days, when the monolayer of cells reached >90% confluency, the mTeSR1 medium was replaced with Roswell Park Memorial Institute Medium (RPMI) 1640 basal medium (ThermoFisher, Waltham, MA) plus 2% B27 without insulin supplement (ThermoFisher) containing 12 µM CHIR99021 (R&D Systems) for 24 h, followed by 5 mM IWP4 (Tocris) for 2 days without medium change. The medium was changed to RPMI 1640 plus B27 complete supplement, and then subsequently the medium was changed every 2 to 3 days. Robust spontaneous beating of the monolayers was observed by day 12**.**

Preparation and design of CRISPR-Cas9 and donor template

The single-guide RNAs (sgRNA) were prepared using online CRISPR tools including CRISPRko Tool from the Broad Institute[24], the CRISPR Finder from Wellcome Trust Sanger Institute[25], and

Benchling[26]. The sgRNA sequences were designed to target the region close to R278 residue of *TNNT2* as shown in **Figure S2**. They were then cloned into a pCCC vector which is based on pSpCas9(BB)-2A-GFP vector (PX458, Addgene plasmid # 48138). The pCCC vector contains the complete U6 promoter for enhanced expression in hiPSCs. The 127 bp asymmetric single-stranded donor nucleotides (ssODNs)[27–29] were designed (**Figure S2**) to include the transitions (T -> A) and (C -> T) that are seen in R278C as well as a silent mutation at the PAM site to prevent the continuous cutting and improve the efficiency of the HDR repair[29].

Transfection and Fluorescence-Activated Cell Sorting (FACS)

Human iPSCs were co-transfected with the R278C-sgRNA-pCCCplasmid and the ssODN donor template using Lipofectamine 3000 (ThermoFisher). Briefly, 2×10^5 hiPSCs were transfected with 500 ng sgRNA plasmid and 10 pmol of ssODN. Since the vector contained GFP as a reporter, the GFP^+ hiPSCs were sorted as single cells using Fluorescence-Activated Cell Sorting (FACS) 48–72 hours post-transfection and were plated on Matrigel-coated plates in mTeSR1[22]. More than 100 single-cell colonies were genotyped. To screen for on-target single mutation, genomic DNA was extracted (DNEasy, Qiagen, Mississauga, ON) and used for PCR amplification of the region around the CRISPR target sites. These amplicons were Sanger sequenced to confirm the single nucleotide mutation at the R278 *TNNT2* site using the primers described in **Figure S2**.

Protein isolation and quantification

The myocardial proteins were isolated from hiPSC-CM pellets (400k-500k cells) for both cell lines approximately 30 days after differentiation. The timely collection of the CMs was done using STEMdiff reagent from the CM dissociation kit (STEMCELL Technologies, Vancouver, BC). STEMdiff was added to each well of hiPSC-CMs, and after incubation with its neutralizing agent, the cells detached from the Geltrex matrix and were pipetted up and down for a homogenous suspension. This was followed by centrifugation of the collected cells to obtain a pellet of hiPSC-CMs. The pellet was then resuspended in lysis buffer according to the number of cells. The cells were counted using the CellDrop automated cell counter (Froggabio, ON). The lysis buffer used contained 100 mM HEPES (pH= 8-8.5) + 20% SDS, and 75 µL of were added per~ 2 million cells. Cell lysates were then placed for 5 minutes in 95°C water bath, followed by 3 minutes on ice. To complete the lysis, the samples were sonicated twice for 30 seconds, and placed on ice between rounds. This was followed by treatment with benzonase (EMD Millipore-Sigma) at 37 °C for 30 min to fragment the chromatin.

After obtaining the CM lysate, each sample was reduced with 10 mM dithiothreitol (DTT) at 37 °C for 30 min, followed by alkylation with 50 mM Chloroacetamide (CAA) for 30 min in the dark. The alkylation was quenched in 50 mM DTT for 10 min at room temperature. To clean the lysates, high-resolution sample-preparation (SP3) technology was the purification approach used to isolate the proteins in the samples. This protocol is a paramagnetic bead–based approach for rapid and efficient processing of protein samples before proteomic analysis[30]. SP3 uses a hydrophilic interaction mechanism for the removal of interfering components (e.g., detergents, salts, buffers, acids, and solvents). The magnetic beads facilitate a wide range of nonselective protein binding that is enabled through the use of an ethanol-driven solvation layer on the surface of the beads. To each sample, hydrophilic and hydrophobic Sera-Mag Speed Beads (GE

Life Sciences, Washington, US) were added in 1:1 ratio. Proteins were then bound to the beads with 100% ethanol (80% v/v) and washed twice with 90% ethanol.

After binding of the proteins to the beads, the samples underwent an overnight enzymatic digestion with trypsin (1:50 w/w), followed by C18 matrix midi-column clean up and elution. The BioPure midi columns (Nest Group Inc.) were conditioned with 200 µL methanol, 200 µL 0.1% Formic Acid (FA), 60% Acetonitrile (ACN), and 200 µL 0.1% Trifluoroacetic Acid (TFA). Samples pH was adjusted to pH=3 – 4 using 10% TFA prior to loading the columns. Samples were sequentially eluted 3 times with 70 µL, 70 µL, and 50 µL 0.1% FA, 60% ACN. The eluate was collected into LoBind tubes and placed into a SpeedVac to remove the organic ACN. Lastly, the samples were re-suspended in 0.1% FA (ready for MS injection). The total protein concentration for each of the purified samples was determined using Nanodrop. Mass spectrometric analyses were performed on Q Exactive HF Orbitrap mass spectrometer coupled with an Easy-nLC liquid chromatography system (Thermo Scientific). This intricate system detects the ionized peptides at the specific time that they elute out of the LC column (retention time). This time is calculated as the period between injection to detection.

In the MS sample chamber (96-well plate), the samples were completely randomized across all conditions and biological replicates. A total of 1 µg peptide per sample was injected for analysis. The peptides were separated over a three-hour gradient consisting of Buffer A (0.1% FA in 2% acetonitrile) and 2%-80% Buffer B (0.1% FA in 95% acetonitrile) at a set flow rate of 300 nL/min. The computerized MS setup produces a pattern spectrum of masses based on the abundance and structure of the detected ionized molecules.

The raw mass-to-charge (M/Z) data acquired from the Q Exactive HF were searched with MaxQuant (MQ)-version 2.0.0.0 (Max Planck Institute, Germany), and Proteome discoverer software (Thermo Fisher Scientific, CA, USA), using the built-in search engine, and embedded standard DDA settings. The false discovery rate for protein and peptide searches was set at 1%. Digestion setting were set to trypsin. Oxidation (M) and Acetyl (N-term) were set as dynamic modifications. Carbamidomethyl (C) was set as fixed modification, and Phosphorylation (STY) was set as a variable modification. For the main comparative protein search, the human proteome database (FASTA) was downloaded from Uniprot (2022_06; 20,365 sequences) and used as the reference file. Common contaminants were embedded from MaxQuant. Peptide sequences that were labeled as “Potential contaminant/REV” were excluded from the final analysis.

Optical mapping for action potential and calcium transient recordings

Prior to imaging, monolayers of hiPSC-CMs ± R278C$^{+/-}$ were perfused with IMDM supplemented with a physiological solution (final concentrations in mM): 140 NaCl, 3.6 KCl, 1.2 $CaCl_2$, 1 $MgCl_2$, 10 HEPES and 5.5 D-glucose for optical mapping as described[22,31,32]. In brief, the cells were incubated with 15 µM of the potentiometric dye RH-237 (Molecular Probes, Eugene, OR) for 45 minutes. After incubating the hiPSC-CMs with RH-237, 5 µM of the Ca^{2+}-sensitive dye Rhod-2AM (Molecular Probes), 20 µM blebbistatin (a myosin ATPase inhibitor (Sigma-Aldrich)) were added to the culture dish. Blebbistatin inhibits contraction and reduces motion artifact with no detectable effect on the electrophysiology properties[14,33]. For imaging, the hiPSC-CMs were excited by 532 nm LEDs. RH-237 and Rhod-2 emissions were monitored using a >710 nm long-

pass and 565-600 nm band-pass filters, respectively, at 100 fps at 37°C. The spectral properties allow both dyes to be fluoresced using 532 nm and their respective emissions to be separated by dichroic mirrors. Both signals were captured with a single Hamamatsu ORCA Flash 4 digital CMOS camera by incorporating an optical image splitter. Electrical field stimulation was applied using stainless steel electrodes placed ~1 cm apart in the imaging chamber. The hiPSC-CMs harboring the *TNNT2* heterozygous mutation R278C$^{+/-}$, and WT were stimulated for 20 seconds each at four stimulation frequencies (55, 65, 75, and 100 beats/min). Data were analyzed using custom-built software in IDL (Exelis Visual Information Solutions, McLean, VA)[22,31,32].

Contractile parameters assessment using SarcTrack

The contractile properties of both hiPSC-CMs ± R278C$^{+/-}$ were studied using SarcTrack[16] about 30 days after differentiation. SarcTrack facilitates high throughput contractile measurements of 2D monolayers of hiPSC-CMs for disease modeling and large-scale pharmaceutical drug screening. This MATLAB algorithm fits each sarcomere to a double wavelet with 6 definable parameters including the distance between wavelet peaks as a function of time, constraint length of each wavelet, width of each individual wavelet, number of angles that wavelet test to find the best fit to the z-disc, distance between grid points to avoid refitting same sarcomere, and the neighborhood around each grid where the best fit for the wavelet pair can be determined. SarcTrack was used to measure the real time contractility of thousands of sarcomeres by running multiple videos in parallel. The images were acquired with a Hamamatsu Orca Flash scMOS camera at 100 frames per second (fps) to measure contractility in hiPSC-CM monolayers cultured on PDMS matrices of 5 kPa tensile strength and stimulated at 1 Hz at 37℃. To image fluorescently labeled sarcomeres, the α-actinin 2-GFP tagged hiPSC-CMs (Allen cell line (AICS-0075)) were used. The images acquired at 100 fps resulted in good signal-to-noise ratio based on a root mean square (RMS) analysis.

On day 14 of differentiation, WT and R278C$^{+/-}$ variant hiPSC-CMs were replated on a Polydimethylsiloxane (PDMS) substrate with a stiffness of 5 kPa to provide a physiological environment for the cells and to increase their maturation. To create a PDMS substrate with 5 kPa elastic modulus, commercially available PDMS, Sylgard 527 gel (equal weights of part A and part B) was used. The surface of PDMS substrate was coated with fibronectin (50 µg/ml) and hiPSC-CMs were seeded with the concentration of 200,000 cell cm^{-2}. Two weeks after replating, the samples were stimulated at 1 Hz frequency and 5 second videos were captured at 100 fps with an ROI of 1024*1024. A Nikon Ti2 microscope was used with 100x oil immersion objective and several videos were captured from different parts of the substrate. Next, by defining appropriate SarcTrack parameters, multiple videos were run simultaneously. To run more than 100 videos at the same time, the files were uploaded to the computational cluster at the Digital Research Alliance of Canada. This advanced research computing system allows one to specify different numbers of CPUs and decreases the computational cost. In this study, 32 CPUs were defined to run more than 100 videos in about 10 hours. The measured contractility parameters included the percentage of sarcomere shortening, time to half contraction, time to half

relaxation, maximum velocity of contraction, and maximum velocity of relaxation of WT and R278C$^{+/-}$ variant hiPSC-CMs. To study the effect of mavacamten on the contractility parameters, R278C$^{+/-}$ variant hiPSC-CMs were treated with 0.3 µM, 1 µM, and 3 µM of mavacamten for 15 min before capturing videos.

Statistical analysis

Average data are provided as mean ± standard error of mean (SEM). The generated MS raw data were filtered and transformed to $\log_2$ scale. This was followed by quantile normalization for all samples. The proteomic profile for the HCM variant was subject to comparative analysis against the isogenic control cell line. The protein groups file obtained from the DDA MQ search was used for all the quantitative statistical analysis based on the detected intensities. All plots, visualizations and statistical comparisons were done using R and Perseus (version 1.6.15.0) software based on unpaired two tailed Student's t-test of significance. The level of significance (p-value < 0.05) and number of data points (n) are indicated in each figure.

RESULTS

Computational potential energy minimization of the wild type and R278C$^{+/-}$ cardiac thin filament

Potential energy minimizations of our Rosetta models were carried out for the cardiac thin filament with and without and the R278C cTnT variant (**Figure 1**). The R278C$^{+/-}$ potential energy minimization analysis suggests that the substitution of a positively charged arginine to a more hydrophobic cysteine may cause more favorable local interactions. The residues in the actin and tropomyosin molecule that are within proximity of residue 278 of cTnT create a slightly positively charged environment. Therefore, the native R278, which is positively charged, may be less favorable to exist in this environment due to the charge repulsion compared to a mutated R278C. If this repulsion of an R278 residue is necessary for normal function (i.e., to provide some flexibility in the local region), we propose that the R278C mutation may disrupt this function due to the lack of the repulsion. In addition, there was no nearby cysteine from actin or Tm that could form any potential disulfide bridges with R278C.

With the cutoff set at 10 Å, five residues of Tm were within the range of the CG or the SG atom for all eight models: Arg167, Val170, Ile171, Ser174 and Arg178 (chain P/W). At this cutoff, the four 6KN7 CG/SG atoms of the models are within range of residues within the closest actin (F/G), whereas the four 6KN8 CG/SG atoms are not within range of any actin molecules. Analysis of this shows that the mutated R278C+/- models of 6KN7 are closer, by about 2 Å, to Arg147 and Thr148 of the actin molecule. Two representations of residue 278 (one in the wildtype actin chain F the second in the variant form) in its environment (with proximal actin/tropomyosin residues labeled) are shown in Figure 1) [34,35].

With the cutoff set at 10 Å, five residues of tropomyosin were within the range of the CG or the SG atom for all eight models: Arg167, Val170, Ile171, Ser174 and Arg178 (chain P/W). At this cutoff, the four 6KN7 CG/SG atoms of the models are within range of residues within the closest actin (F/G), whereas the four 6KN8 CG/SG atoms are not within range of any actin molecules. Analysis of this shows that the mutated R278C$^{+/-}$ models of 6KN7 are closer, by about 2 Å, to Arg147 and Thr148 of the actin molecule. Two representations of residue 278 (one in the wildtype actin chain F the second in the variant form) in its environment (with proximal actin/tropomyosin residues labeled) are shown in **Figure 1**)[34,35].

Ca^{2+} sensitivity and dissociation rates of the human cardiac reconstituted thin filaments (hcRTF)

Steady-state fluorescence measurements were carried out on WT and variant hcRTFs, and Ca^{2+}-dependent IAANS fluorescence increase was observed for all hcRTF constructs. The R278C$^{+/-}$ variant showed a statistically significant increase of Ca^{2+} sensitivity by ~2.3 fold ($p \leq 0.05$) (**Figure 2**).

Stopped-flow fluorescence spectroscopy was used to determine the Ca^{2+} dissociation rates from the hcRTF constructs. Upon the addition of EGTA, the Ca^{2+} rapidly dissociated from cTnC, inducing a cTnC conformational change in which the fluorescence change was recorded. As Ca^{2+} was stripped from cTnC by EGTA, a decrease in IAANS fluorescence was observed for all hcRTF

constructs. The hcRTF harboring R278C$^{+/-}$ TnT variant shows a significant decrease of k_{off} compared to WT, increasing the Ca^{2+} sensitivity significantly by ~1.4 fold ($p \leq 0.05$) (**Figure 2**). This explains, at least in part, the increase of Ca^{2+} sensitivity conferred by the hcRTF harboring *TNNT2* mutation in the steady-state experiments.

Protein quantification and PTM characterization using mass spectrometry

To further investigate the variant-related deviations, we obtained the full proteomic profile of R278C$^{+/-}$ *TNNT2* hiPSC-CMs in comparison to WT *TNNT2* hiPSC-CMs as the isogenic control using bottom-up mass spectrometry.

We found 102 of 2327 proteins to be statistically (1% FDR) more abundant in WT and 198 proteins to be more abundant in R278C$^{+/-}$ cells (**Figure 3A**). Next, we examined individual proteins of interest involved in control of contractility, structural integrity, metabolism, and crucial cardiac remodeling pathways (**Figure 3B-D**). The variable profile was further probed among individual protein groups. Even though no significant difference was noted in most sarcomeric proteins, the myosin heavy chain showed a dissimilarity between the R278C$^{+/-}$ *TNNT2* and the isogenic control hiPSC-CMs. As seen in **Figure 3B**, the dominant form of myosin heavy chains (MHC), Myosin Heavy chain 7 (MYH7; βMHC) with relatively slow ATPase activity, did not exhibit any quantitative changes between the two groups. However, the other key paralog, MYH6 (αMHC) with relatively fast ATPase activity, was significantly over-expressed in the R278C$^{+/-}$ *TNNT2* hiPSC-CMs. Also, the myosin light chains (MYLs), particularly MYL2, showed a significant decrease in the R278C-harboring CMs relative to the wildtype cells (**Figure 3B**).

Proteins important for the structural integrity and organization of the Z-disc, such as α actinin (ACTN1), also showed variable translational profiles between the R278C$^{+/-}$ and WT CMs. Early change in the diastolic compliance is suggested by the significant increase in tubulin β-4B chain (*TUBB4B*) (**Figure 3C**). Moreover, other structural components responsible for the overall integrity of the cardiomyocyte, such as desmin and junctophilin, were detected with significantly lower intensities in the R278C$^{+/-}$ CMs (**Figure 3D**).

Lastly, as shown in **Figure 4**, a metabolic shift in the proteomic profile was observed in the R278C$^{+/-}$ CMs, in which glycolytic proteins were significantly up-regulated (e.g. insulin-independent glucose transporter protein type 1 (GLUT1)), β-oxidation proteins were significantly down-regulated (e.g., Acyl-CoA dehydrogenase (ACADS)), and proteins responsible for efficient energy production were significantly decreased (e.g. Creatine kinase (CKM)).

Besides the differences in protein quantities, significant alterations between the two groups on the post translational level, particularly phosphorylation (**Figure 5**), were observed. This figure shows the major pathways that were affected post-translationally by this variant. For example, the NFAT-Calcineurin pathway is a major contributor to pathological cardiac remodeling. A significant dephosphorylation of the key signaling component NFATC2 was detected in the R278C$^{+/-}$ *TNNT2* hiPSC-CMs. Furthermore, phosphorylation of important regulatory components that facilitate contractility, such as MYL2 and MYBPC3, were significantly increased (**Figure 5**).

Optical mapping (OM) to measure voltage and Ca^{2+} transients in 2D monolayers of hiPSC-CMs

Using OM on 2D monolayers of hiPSC-CMs ± R278C$^{+/-}$, we investigated the effect of various stimulation frequencies on the membrane voltage (V_m) and cytosolic Ca^{2+} transients. V_m and Ca^{2+} transients were determined from the fluorescence emitted by RH-237 and Rhod-2, respectively. **Figure 6, Panel A** shows representative traces of V_m and Ca^{2+} transients from monolayers of hiPSC-CMs electrically stimulated at 55 and 65 bpm. The action potential and Ca^{2+} transients are shown for both WT (A1, A2) and R278C$^{+/-}$ (A4, A5) hiPSC-CMs and both groups entrained normally to these stimulation frequencies. In panels A3 and A6, the field stimulation rate was increased to 100 bpm. While the WT hiPSC-CMs showed normal entrainment to this stimulation frequency (Panel A3), R278C$^{+/-}$ hiPSC-CMs (**Panel A6**) developed an alternans-like irregular and arrhythmogenic voltage and Ca^{2+} transients at this frequency. None of the WT hiPSC-CM monolayers exhibited abnormal V_m or Ca^{2+} transients at 100 bpm.

The action potential duration at 30% (APD_{30} **Figure 6 Panel B1**) and 80% (APD_{80} **Figure 6 Panel B2**) repolarization were determined as a function of stimulation frequency (55, 65, and 75 bpm) in both WT and R278C$^{+/-}$*TNNT2* hiPSC-CMs (black and red, respectively) These frequencies were chosen because 55 bpm was higher than the intrinsic beating rate and 75 bpm was below frequencies that induced any observable form of arrhythmia.

Subsequently, the response of WT and R278C$^{+/-}$ *CMs* with respect to Ca^{2+} transient duration at 30% ($CaTD_{30}$) and 80% ($CaTD_{80}$) repolarization at 55, 65, and 75 bpm field-stimulation frequencies is shown in **Figure 6C**. $CaTD_{30}$ was significantly prolonged in R278C$^{+/-}$ hiPSC-CMs compared to WT hiPSC-CM at all three stimulation frequencies (**Figure 6C1**). In R278C$^{+/-}$ *TNNT2* hiPSC-CMs, $CaTD_{80}$ was prolonged significantly ($p < 0.05$) compared to WT *TNNT2* hiPSC-CMs at 65 bpm and 75 bpm (**Figure 6C2**).

Restitution of Action Potential Duration (APD) and Ca^{2+} Transient Duration (CaTD)

As shown in **Figure 6**, WT hiPSC-CMs show both action potential duration and Ca^{2+} transient shortening over this range (55-75 bpm) of stimulation frequencies consistent with the concept of restitution. However, R278C$^{+/-}$ hiPSC-CMs did not exhibit any indication of APD shortening under these experimental conditions, but did, however, display significantly ($p \leq 0.05$) shorter Ca^{2+} transient durations as reflected by reduced $CaTD_{30}$ and APD_{80} at 75 vs. 55 bpm.

SarcTrack Analysis

The goodness of double wavelet fitting to the sarcomere is shown in **Figure 7A**.The contractile parameters were measured while the 2D monolayer of hiPSC-CMs was paced at 1 Hz and maintained at 37 ^{o}C. The percentage of maximal sarcomere shortening was significantly higher for R278C$^{+/-}$ (14.1 ± 0.5) compared to the WT (12.8 ± 0.9) hiPSC-CMs (**Figure 7C**). Dramatic increases in the time-to-half maximal contraction and relaxation were also observed in R278C$^{+/-}$ compared to WT hiPSC-CMs (**Figures 7**), which reflected the hypercontractility of R278C$^{+/-}$ variant. However, no significant changes were observed in either the maximum velocity of the relaxation or contraction (**Figure 7B**). We next investigated the effect of different concentrations of mavacamten on the contraction and relaxation parameters of the R278C$^{+/-}$ hiPSC-CMs. **Figure**

8A shows a significant decrease in the maximum velocity of contraction and the maximum percentage of sarcomere shortening of R278C$^{+/-}$ hiPSC-CMs after adding 0.3, 1, and 3 µM mavacamten. **Figure 8B** shows that 1 µM and 3 µM mavacamten significantly decreased the maximum velocity of relaxation of R278C$^{+/-}$ hiPSC-CMs.

Discussion

Potential energy minimization simulations of the cardiac thin filament

Due to the highly flexible nature of cTnT, the molecular structure of most regions of cTnT remain unsolved except for residues 199-272 that are included in the high-resolution troponin core domain crystal structure (PDB: 4Y99)[34] and recently determined thin filament cryo-EM structures (PDB: 6KN7, PDB: 6KN8). The potential energy minimization data for R278C$^{+/-}$ suggests that the cysteine may experience slightly less charge repulsion with nearby residues from actin and Tm. As shown in Figure 1, these nearby residues in actin,1 and Tm create a positively charged microenvironment. We speculate that the charge repulsion between the positively charged native R278 and the local environment might be necessary for its normal function, in which the inherent dynamics and flexibility is required for the molecular movement that is propagated along the thin filament in response to the Ca^{2+} binding to and dissociation from the troponin complex.

Ca^{2+} binding analysis using steady-state and stopped flow fluorescence spectroscopy

Somewhat unanticipated results arose from the changes in the Ca^{2+} sensitivity and kinetics associated with the R278C$^{+/-}$ variant in the adult hcRTF (**Figure 2**). Although transgenic mice expressing the R278C$^{+/-}$ variant show no change in myofilament Ca^{2+} senstivity[11,14], our data show that the variant causes a similar magnitude of Ca^{2+} sensitization using human models of both steady-state and pre-steady state kinetic data (**Figure 2**). This striking difference could be due to: 1) the species differences between the rodent and human; 2) the experimental model (skinned cardiomyocytes vs hcRTFs) or 3) the fact that the mice used in these studies were 3-4 months old and may have been too young to develop the pathophysiological phenotypes associated with the sometimes late-onset pathology associated with this variant[12].

Human induced pluripotent stem cells-derived cardiomyocytes (hiPSC-CMs) studies

We used genome editing (CRISPR/Cas9) to generate heterozygous R278C$^{+/-}$ *TNNT2* hiPSCs. This technique enabled us to compare R278C$^{+/-}$ *TNNT2* hiPSCs with the isogenic control hiPSCs instead of comparing it with another control hiPSCs that have different genetic and epigenetic backgrounds. Every precaution was taken to ensure that the WT and R278C$^{+/-}$ TNNT2 variant hiPSC-CMs were as similar as possible except for the point mutation. Both lines were exposed to the CRISPR/Cas9 genome-editing protocol with the R278C$^{+/-}$ line undergoing a double-strand break and then homology-directed repair while the WT remained unchanged. The 10 most likely off-target mutation sites were all sequenced to determine that this was not a contributing factor. Both lines were then subjected to identical differentiation protocols in parallel.

Proteomic profile of R278C$^{+/-}$ hiPSC-CMs

To further emphasize the molecular changes caused by the R278C$^{+/-}$ *TNNT2* variant, we explored the proteomic profile of both cell lines using shotgun MS to perform peptide to protein identification and quantification. The muscle thick filaments' main motor protein group is called myosin heavy chain (MYH). Most species develop many temporally and spatially controlled muscle MYH paralogs. This implies that diverse MYH paralog features are required for

determining contractility qualities. For example, the myosin α heavy chain (*MYH6*) has fast twitch mechanics response to excitation-contraction coupling, while β-myosin heavy chain (*MYH7*) has a slower but more powerful stroke[36]. Therefore, the detected increase in MYH6 expression (**Figure 3B**), could be a result of increased contractility and cross bridge interactions with the thin filament because of the increased myofilament calcium sensitivity.

Myosin light chain-2 (*MYL2*/MLC-2) is a major sarcomeric protein in the mammalian cardiac muscle, it is also referred to as the regulatory light chain (RLC) of the contractile unit. MYL2 plays an important role in embryonic heart muscle structure and function, its phosphorylation regulates cardiac myosin cycling kinetics, rotation, and contractility[37]. **Figure 3B** reflects the abundance levels of MYL2 R278C$^{+/-}$ CMs, respectively, compared to the isogenic controls. A significant decrease in MYL2 expression levels has been recorded for the *TNNT2* variant. This deviation could be attributed to the increased calcium sensitivity instigated by the HCM-causing mutations. The hypersensitive myofibrils result in prolonged crossbridge formation, which in turn may result in a disrupted need for regulation by MYL2, leading to a negative response of decreased expression in the variants[38] (**Figure 3B**).

The expression levels of the slow skeletal isoform of troponin I (*TNNI1*) were detected in higher intensity than the cardiac isoform (*TNNI3*) in both WT and R278C$^{+/-}$ CMs (Figure 3B). This dominance of the *TNNI1* isoform is a major indicator that the hiPSC-CMs lack maturity and remain early in development[39]. The mean ratio of TNNI3/TNNI1 is displayed in Table 1.

Table 1: Average intensity of the slow skeletal (*TNNI1*) and the cardiac (*TNNI3*) troponin 1 paralogs.

Average intensity	***WT***	***R278C***
TNNI1	32.41	31.75
TNNI3	24.69	25.34
TNNI3/TNNI1	0.76	0.80

The Z-disc is a protein-rich structure that acts to tether the thin filaments in the sarcomeres. Proteins of the Z-disc are integral for maintaining the architectural integrity of the sarcomere. They also enable it to function as a mechanical signaling center. Numerous proteins interact in the Z-disc to facilitate force transduction and intracellular signaling in cardiac muscle. In this study, many proteomic alterations were found to be directly or indirectly associated with Z-disc disorganization and myofibrillar disarray. The presence of mechanical strain on the Z-disc may lead to altered transcriptional regulation through mechanosensitive pathways, affecting the expression profile of several downstream proteins, such as the myosins[40,41]. As shown in **Figure 3 panel C** the R278C$^{+/-}$ CMs show prominent Z-disc modifications in a consistent fashion. α-actinin is a major protein found in the Z-disc and is involved in the crosslinking of actin filaments. α-actinin also interacts with titin to form a scaffold for large protein complexes[42]. During the pathogenic manifestation of cardiomyopathies, such as HCM, an upregulation of α-actinin is

expected due to the increased mechanical stiffness of the CM[42]. In **panel 3C**, the expression levels of α-actinin1 (*ACTN1*) show a significant increase compared to the isogenic control CMs. On the other hand, protein groups responsible for the structural integrity and stability of the Z-disc, such as MYOZ2 (Myozenin2), NEBL (Nebulette), and SMPX (small muscle protein)[42,43] were significantly downregulated in R278C$^{+/-}$ CMs, which indicates a further exacerbation of the Z-disc inflexibility and disorganization. Also, other interacting non-sarcomeric cytoskeletal components, such as microtubules, play a crucial role in signal transduction and contractility. Therefore, there is a growing interest in exploring the role of microtubules in affecting diastolic compliance[44]. As shown in Figure 3 panel C, TUBB4B is significantly increased in R278C$^{+/-}$ relative to the isogenic control. This upregulation could be indicative of elevated tubulin polymerization and stabilization, which is an early pathological adaptive response in cardiomyopathies and heart failure that can induce stiffness which directly affects the diastolic compliance of the cell.

Moreover, other structural components that function in sarcomeric protein crosslinking and assembly demonstrate a consistent decline in protein expression in the R278C$^{+/-}$ CMs relative to the isogenic control CMs. Examples of such proteins are shown in **Figure 3 panels C and D**, which include *NEBL* (Nebulette)- which functionally links sarcomeric actin to the desmin intermediate filaments in the sarcomeres[45], *JPH2* (Junctophilin2)- provides a structural bridge between the plasma membrane and the sarcoplasmic reticulum and is required for normal excitation-contraction coupling in cardiomyocytes [46], *OBSCN* (Obscurin)- highly involved in the assembly of myosin into sarcomeric A bands[47], *FHL 1&2* (Four and a half LIM domains)- negatively regulate the calcineurin/NFAT signaling pathway in cardiomyocytes[48], and *DES* (Desmin)- a key structural intermediate filament required for maintaining normal structure of sarcomeres and interconnecting the Z-disks[49]. Based on these findings, the significant decrease discovered in these protein groups could be a strong indication for some underlying serious structural remodeling transpiring[50].

From a metabolic standpoint, other significant expression differences were discovered in key glycolysis and energy production-related proteins. *SLC2A1* or *GLUT1* (Solute carrier family 2, facilitated glucose transporter member 1) is one of the main transporters that brings in extracellular glucose for metabolic use[51]. We speculate that the hiPSC-CMs harboring a *TNNT2* variant undergo a switch to the fetal metabolic program, which heavily depends on glycolysis for ATP generation. It has been shown in many studies that in failing and hypertrophic hearts, the switch to the fetal metabolic gene profile is done by downregulating adult gene transcripts rather than by upregulating the fetal genes[52,53]. The main source of energy in the post-natal cardiac muscle relies on the metabolism of fatty acids. Key proteins involved in this oxidative pathway include short, medium, and long- chain specific acyl-CoA dehydrogenases. These enzymes are responsible for catalyzing the first step of mitochondrial beta-oxidation, which leads to the breakdown of fatty acids into acetyl-CoA thus allowing for the production of energy from fats[52].

In this study, several glycolysis-related proteins were detected in higher quantities relative to the major proteins involved in fatty acid oxidation. The data reflects a significant down-regulation in

the β-oxidation pathway. For example, facilitated glucose transporter member 1 (*GLUT1*), ATP-dependent 6-phosphofructokinase, muscle type (*PFKAM*), and phosphoglycerate mutase 1 (*PGAM1*) were all increased in the R278C$^{+/-}$ samples relative to their isogenic control cells (**Figure 4**). However, major fatty-acid metabolism proteins, such as short-chain specific acyl-CoA dehydrogenase (*ACADS*), medium-chain specific acyl-CoA dehydrogenase (*ACADM*), and heart fatty acid-binding protein (*FABPH*) were significantly down-regulated in the HCM-variant (**Figure 4**). This provides further evidence for the manifestation of the switch to the fetal gene program. This findings both coincide and differ with those found by Gilda et al[50] in a 3 month old transgenic mouse model in which the R278C overexpression caused increased AMP levels indicating metabolic stress yet also decreased glycolysis related proteins.

Another major metabolic hallmark of cardiac pathology is a notable reduction of *CKMT2* (mitochondrial creatine kinase) / *CK* (creatine kinase) ratios in pre-hypertrophic patients. This observed decrease is a direct reflection of impaired energetics and inefficient ATP utilization in failing and hypertrophic hearts. Similarly, the HCM-related impaired sarcomere energetics may provoke mitochondrial dysfunction, reduced ATP production, and increased reactive oxygen species (ROS) generation. All these indices are directly related to a potential pathogenic decline in the rate of the electron transport chain, leading to lower amounts of respiratory complex proteins[54,55]. As displayed in **Figure 4**, CKM (creatine kinase) and CKMT2 (mitochondrial creatine kinase) are both significantly decreased in the R278C$^{+/-}$ cell line. Moreover, the results show a potential hint for reduced mitochondrial content and energy production through the electron transport chain.

Post-translational modifications (PTMs) related to HCM progression in R278C$^{+/-}$ hiPSC-CMs

To further examine the potential for contractility changes within the proteomic findings, the phosphorylation profile alterations among WT, and R278C$^{+/-}$ hiPSC-CMs were quantified using MS. Cardiac contractility is regulated by numerous factors including the phosphorylation of sarcomeric proteins. In relaxed heart muscle there is evidence for a population of myosin cross-bridges with the two heads in an interacting motif (IHM) to establish a so-called super relaxed state (SRX) with low ATPase activity and sequestered from interacting with the thin filaments[56]. Another population of cross-bridges exists in a disordered relaxed (DRX) state with swaying free heads poised to interact with the thin filaments, hydrolyze ATP, and induce force generation and shortening with calcium activation. In healthy and relaxed human hearts, it is proposed that the majority of myosin heads exist in the SRX state but in pathological conditions like HCM, the IHM state of myosin is disturbed and the percentage of DRX is increased[56]. It has been hypothesized that phosphorylation of myosin binding protein-C (MyBPC3) and myosin regulatory light chain (MYL2) may promote the DRX state by recruitment of sequestered IHM heads[56]. Evidence for the favored transition to the DRX state is shown in **Figure 5**, where an increased number of phosphorylated peptides exist in *MYBPC3* and *MYL2* at sites Ser284 and Ser15, respectively.

The shortening velocity may also be further affected with the increased phosphorylation of MYBPC3 at Ser284. In a transgenic mouse model, it has been previously shown that MYBPC3 phosphorylation could change both filament orientation and mechanics of contractility by

modulation of the myosin heads SRX state, although no direct effect was observed on Ca^{2+} sensitivity [57].

The effect of oxidative stress can also be studied on the PTM level. Important modifications occur in response to increased ROS production including S-glutathionylation[58]. Due to the nature of the TNNT2 variant, the substitution of arginine (R) with a cysteine (C) introduces a novel residue for a possible S-glutathionylation. One of the major future aims of this study is to explore the modifications on the C278 residue, particularly, S-glutathionylation. It has been previously shown that S-glutathionylation of various sarcomeric proteins is involved in the mechanical modulation of contractility in relation to changes in the oxidative state of the cell[58].

All in all, the proteomic variability between the two groups provides clear evidence of a pathogenic manifestation taking place in early stages of development in cardiomyocytes carrying the R278C$^{+/-}$ *TNNT2* variant.

Functional studies

The effect of R278C$^{+/-}$ *TNNT2* variant on voltage and Ca^{2+} transients at different stimulation frequencies (**Figure 6**) was examined using optical mapping of 2D monolayers of hiPSC-CMs. Although the mechanism of arrhythmogenesis is not clear, alterations in Ca^{2+}-handling properties are likely involved. Tachycardia in HCM patients carrying *TNNT2* variants can be arrhythmogenic. In this regard, the rapid heart rate resulted in atrial fibrillation or sinus tachycardia in over 90% of the arrhythmic episodes in HCM patients who were recipients of implantable cardiac defibrillators (ICDs)[59]. Moreover, sinus tachycardia was observed in 90% of ventricular fibrillation episodes in HCM affected children who were treated with heart rate therapeutics[59]. The results of these studies are consistent with the high incidence of ventricular tachycardia and sudden cardiac death possibly linked to high Ca^{2+} sensitivity due to cTnT mutations[7,60,61]. Our results in R278C$^{+/-}$ CMs demonstrate that fast stimulating rates can be arrhythmogenic, compared to WT *TNNT2* hiPSC-CM (**Figure 6**).

As shown in the SarcTrack data in **Figure 7**, the R278C$^{+/-}$ variant enhances contractility as reflected by increasing the maximum sarcomere shortening but also increases the time to half maximal contraction, and time to half maximal relaxation. These findings are probably related to the prolonged Ca^{2+} transients shown in **Figure 6**. Based on the proteomic results, a reduction in the SRX myosin due to the cMyBP-C and MYL2 phosphorylation may be regarded as a possible mechanism for increased contractility in R278C$^{+/-}$ hiPSC-CMs[56]. However, further studies are required to assess the underlying mechanisms of increased contraction in *TNNT2* variants. The efficacy of mavacamten for treating HCM causing R278C$^{+/-}$ variants was assessed. The results showed that mavacamten regulated contractility by decreasing the sarcomere shortening as well as decreasing the velocity of contraction and relaxation.

Previous studies in murine cTnT-linked HCM mutations have identified the increased Ca^{2+} sensitivity in the cardiac skinned fibers and decreased Ca^{2+} dissociation rate ($k_{off\,(Ca)}$) from cardiac troponin C during diastole[13–15,62,63]. However, the total number of Ca^{2+}-binding sites was not

altered in cTnT mutations. Therefore, increased Ca^{2+} sensitivity due to cTnT variants increases cytosolic Ca^{2+} buffering; this is because the troponin complex accounts for a substantial portion of cytosolic Ca^{2+} buffering[63,64]. During diastole, increased Ca^{2+} sensitivity results in the prolongation of Ca^{2+} transient and slower Ca^{2+} decay rate. In previous studies[65,66], a theory for the mechanism of intracellular Ca^{2+} alternans was developed. It is called the "3R" theory since Ca^{2+} alternans is promoted by the interactions of random firing of the Ca^{2+} sparks, recruitment of neighboring Ca^{2+} release units (CRUs) for firing (spark-induced sparks), and refractoriness of the CRUs. The recruitment is determined by the coupling strength between CRUs, and Ca^{2+} buffering is one of the parameters affecting recruitment[67]. In this mechanism, Ca^{2+} alternans is promoted by the enhancement of the recruitment[66]. This theory can provide a plausible mechanism for the alternans promoted by the R278C$^{+/-}$ variant that was observed in these experiments. The increased thin filament Ca^{2+} sensitivity appears to be due primarily to the decrease in the Ca^{2+} off rate constant. This reduction/slow-down of the unbinding rate of Ca^{2+} from the myofilament effectively reduces the Ca^{2+} buffering effect which can promote Ca^{2+}alternans based on the "3R" theory[65–67].

This study was a serious effort to uncover the proteomic and functional alterations in the early stages of R278C HCM on a broad scale using an unbiased approach. Despite that, several limitations arose that could be improved in future experiments. Firstly, the protein purification protocol is based on a magnetic bead-based solvation layer that captures mostly hydrophilic proteins or soluble portions of proteins. This presents a limitation in studying hydrophobic or membrane-bound proteins (e.g., ion channels). Secondly, functional studies were conducted with only hiPSC-derived cardiomyocytes in the2D monolayers. As it is known that a 3D structure that includes fibroblasts and endothelial cells, for example, could contribute to the clinical phenotype.

Conclusions

The R278C$^{+/-}$ *TNNT2* variant was generated in hiPSC-CMs using CRISPR/Cas9 and the pathological consequences of this variant on the proteome and function of hiPSC-CMs was studied. Our findings are indicative of potential pathological remodeling in R278C$^{+/-}$ vs. the isogenic control occurring in the early developmental stages of life. Hypercontractility was observed in R278C$^{+/-}$ hiPSC-CMs and the mavacamten was found to be a potential therapeutic agent for this specific variant. Furthermore, an increase in Ca^{2+} sensitivity was observed in the R278C$^{+/-}$ hcRTF model. Lastly, the alteration of AP and Ca^{2+} handling in R278C$^{+/-}$ CMs was shown to be proarrhythmic at higher stimulation frequencies using optical mapping. Remarkably, the proteome and contractility were dramatically impacted by the insertion of a point mutation in one allele of troponin T and likely has profound consequences in the disease phenotype.

The hiPSC-CMs along with the genome-editing tools demonstrate the utility of this technology for modeling HCM-linked sarcomeric mutations, identifying the arrhythmogenic factors, and potential developing therapeutic agents for the treatment of HCM.

Author contributions :

SS Experimental: genome editing ; hiPSC differentiation ; optical mapping
AYL Experimental: recombinant protein expression, reconstituted cardiac thin filaments
FJ Experimental: hiPSC differentiation, hiPSC-CM protein extraction, MS proteomics
YM Experimental: hiPSC differentiation; SarcTrack analyses
HH Expertise in hiPSC-CM maturation
DHB Expertise in microtubules
TB Experimental: genome editing
MG Experimental: transcriptomic data
BR Experimental: genome editing
SJ Experimental: PDMS matrix design and fabrication
RN
AC Experimental: Potential energy minimization simulations of the cardiac thin filament
PL Data analysis – thin filament expertise
RJS troponin structure and function expertise
CT SarcTrack expertise
SL Potential energy minimization simulations of the cardiac thin filament
PL MS proteomics expertise
GFT PI on project, grant holder, project designer and coordinator

Competing interests. R.J.S. is a member of the Scientific Advisor Board of Cytokinetics, Inc. and a consultant to Myokardia/Bristol- Myers-Squibb.

References

1. Maron, B. J. *et al.* Prevalence of hypertrophic cardiomyopathy in a general population of young adults. Echocardiographic analysis of 4111 subjects in the CARDIA Study. Coronary Artery Risk Development in (Young) Adults. *Circulation* **92**, 785–789 (1995).
2. Maron, B. J. *et al.* Contemporary Definitions and Classification of the Cardiomyopathies. *Circulation* **113**, 1807–1816 (2006).
3. Elliott, P. M. *et al.* Sudden death in hypertrophic cardiomyopathy: identification of high-risk patients. *J Am Coll Cardiol* **36**, 2212–2218 (2000).
4. Maron, B. J. Hypertrophic cardiomyopathy: a systematic review. *JAMA* **287**, 1308–1320 (2002).
5. Tester, D. J. & Ackerman, M. J. Cardiomyopathic and channelopathic causes of sudden unexplained death in infants and children. *Annu Rev Med* **60**, 69–84 (2009).
6. Messer, A. E. *et al.* Mutations in troponin T associated with Hypertrophic Cardiomyopathy increase Ca^{2+}-sensitivity and suppress the modulation of Ca^{2+}-sensitivity by troponin I phosphorylation. *Arch Biochem Biophys* **601**, 113–120 (2016).
7. Knollmann, B. C. & Potter, J. D. Altered regulation of cardiac muscle contraction by troponin T mutations that cause familial hypertrophic cardiomyopathy. *Trends Cardiovasc Med* **11**, 206–212 (2001).
8. Maron, B. J. *et al.* Diagnosis and Evaluation of Hypertrophic Cardiomyopathy: JACC State-of-the-Art Review. *Journal of the American College of Cardiology* **79**, 372–389 (2022).
9. Eschenhagen, T., Mummery, C. & Knollmann, B. C. Modelling sarcomeric cardiomyopathies in the dish: from human heart samples to iPSC cardiomyocytes. *Cardiovasc Res* **105**, 424–438 (2015).
10. Schuldt, M. *et al.* Mutation location of HCM-causing troponin T mutations defines the degree of myofilament dysfunction in human cardiomyocytes. *J Mol Cell Cardiol* **150**, 77–90 (2021).
11. Knollmann, B. C. *et al.* Familial hypertrophic cardiomyopathy-linked mutant troponin T causes stress-induced ventricular tachycardia and Ca^{2+}-dependent action potential remodeling. *Circ Res* **92**, 428–436 (2003).
12. Hernandez, O. M. *et al.* F110I and R278C Troponin T Mutations That Cause Familial Hypertrophic Cardiomyopathy Affect Muscle Contraction in Transgenic Mice and Reconstituted Human Cardiac Fibers *. *Journal of Biological Chemistry* **280**, 37183–37194 (2005).
13. Shafaattalab, S. *et al.* Mechanisms of Arrhythmogenicity of Hypertrophic Cardiomyopathy-Associated Troponin T (TNNT2) Variant I79N. *Frontiers in Cell and Developmental Biology* **9**, (2021).
14. Baudenbacher, F. *et al.* Myofilament Ca^{2+} sensitization causes susceptibility to cardiac arrhythmia in mice. *J Clin Invest* **118**, 3893–3903 (2008).
15. Schober, T. *et al.* Myofilament Ca sensitization increases cytosolic Ca binding affinity, alters intracellular Ca homeostasis, and causes pause-dependent Ca-triggered arrhythmia. *Circ Res* **111**, 170–179 (2012).

16. Toepfer, C. N. *et al.* SarcTrack. *Circulation Research* **124**, 1172–1183 (2019).

17. Olivotto, I. *et al.* Mavacamten for treatment of symptomatic obstructive hypertrophic cardiomyopathy (EXPLORER-HCM): a randomised, double-blind, placebo-controlled, phase 3 trial. *Lancet* **396**, 759–769 (2020).

18. Yamada, Y., Namba, K. & Fujii, T. Cardiac muscle thin filament structures reveal calcium regulatory mechanism. *Nat Commun* **11**, 153 (2020).

19. Alford, R. F. *et al.* The Rosetta All-Atom Energy Function for Macromolecular Modeling and Design. *J Chem Theory Comput* **13**, 3031–3048 (2017).

20. Wang, C., Bradley, P. & Baker, D. Protein-protein docking with backbone flexibility. *J Mol Biol* **373**, 503–519 (2007).

21. Coulton, A., Lehrer, S. S. & Geeves, M. A. Functional Homodimers and Heterodimers of Recombinant Smooth Muscle Tropomyosin. *Biochemistry* **45**, 12853–12858 (2006).

22. Shafaattalab, S. *et al.* In vitro analyses of suspected arrhythmogenic thin filament variants as a cause of sudden cardiac death in infants. *Proc Natl Acad Sci U S A* **116**, 6969–6974 (2019).

23. Davis, J. P. *et al.* Effects of Thin and Thick Filament Proteins on Calcium Binding and Exchange with Cardiac Troponin C. *Biophysical Journal* **92**, 3195–3206 (2007).

24. sgRNA Designer: CRISPRko. https://portals.broadinstitute.org/gpp/public/analysis-tools/sgrna-design.

25. Hodgkins, A. *et al.* WGE: a CRISPR database for genome engineering. *Bioinformatics* **31**, 3078–3080 (2015).

26. CRISPR gRNA Design Tool | Benchling. https://www.benchling.com/crispr.

27. Ran, F. A. *et al.* Double nicking by RNA-guided CRISPR Cas9 for enhanced genome editing specificity. *Cell* **154**, 1380–1389 (2013).

28. Ran, F. A. *et al.* Genome engineering using the CRISPR-Cas9 system. *Nat Protoc* **8**, 2281–2308 (2013).

29. Richardson, C. D., Ray, G. J., DeWitt, M. A., Curie, G. L. & Corn, J. E. Enhancing homology-directed genome editing by catalytically active and inactive CRISPR-Cas9 using asymmetric donor DNA. *Nat Biotechnol* **34**, 339–344 (2016).

30. Hughes, C. S. *et al.* Single-pot, solid-phase-enhanced sample preparation for proteomics experiments. *Nat Protoc* **14**, 68–85 (2019).

31. Shafaattalab, S. *et al.* Ibrutinib Displays Atrial-Specific Toxicity in Human Stem Cell-Derived Cardiomyocytes. *Stem Cell Reports* **12**, 996–1006 (2019).

32. Gunawan, M. G. *et al.* Drug screening platform using human induced pluripotent stem cell-derived atrial cardiomyocytes and optical mapping. *Stem Cells Transl Med* **10**, 68–82 (2021).

33. Kovács, M., Tóth, J., Hetényi, C., Málnási-Csizmadia, A. & Sellers, J. R. Mechanism of blebbistatin inhibition of myosin II. *J Biol Chem* **279**, 35557–35563 (2004).

34. Marston, S. & Zamora, J. E. Troponin structure and function: a view of recent progress. *J Muscle Res Cell Motil* **41**, 71–89 (2020).

35. Takeda, S., Yamashita, A., Maeda, K. & Maéda, Y. Structure of the core domain of human cardiac troponin in the Ca(2+)-saturated form. *Nature* **424**, 35–41 (2003).

36. Walklate, J. *et al.* Alpha and beta myosin isoforms and human atrial and ventricular contraction. *Cell. Mol. Life Sci.* **78**, 7309–7337 (2021).

37. Sheikh, F., Lyon, R. C. & Chen, J. Functions of Myosin Light Chain-2 (MYL2) In Cardiac Muscle and Disease. *Gene* **569**, 14–20 (2015).

38. Markandran, K., Poh, J. W., Ferenczi, M. A. & Cheung, C. Regulatory Light Chains in Cardiac Development and Disease. *Int J Mol Sci* **22**, 4351 (2021).

39. Hunkeler, N. M., Kullman, J. & Murphy, A. M. Troponin I isoform expression in human heart. *Circ Res* **69**, 1409–1414 (1991).

40. Rysä, J., Tokola, H. & Ruskoaho, H. Mechanical stretch induced transcriptomic profiles in cardiac myocytes. *Sci Rep* **8**, 4733 (2018).

41. Lyon, R. C., Zanella, F., Omens, J. H. & Sheikh, F. Mechanotransduction in cardiac hypertrophy and failure. *Circ Res* **116**, 1462–1476 (2015).

42. Wadmore, K., Azad, A. J. & Gehmlich, K. The Role of Z-disc Proteins in Myopathy and Cardiomyopathy. *Int J Mol Sci* **22**, 3058 (2021).

43. Wang, H. *et al.* Mutations in NEXN, a Z-disc gene, are associated with hypertrophic cardiomyopathy. *Am J Hum Genet* **87**, 687–693 (2010).

44. Caporizzo, M. A., Chen, C. Y., Bedi, K., Margulies, K. B. & Prosser, B. L. Microtubules Increase Diastolic Stiffness in Failing Human Cardiomyocytes and Myocardium. *Circulation* **141**, 902–915 (2020).

45. Perrot, A. *et al.* Mutations in NEBL encoding the cardiac Z-disk protein nebulette are associated with various cardiomyopathies. *Arch Med Sci* **12**, 263–278 (2016).

46. Beavers, D. L., Landstrom, A. P., Chiang, D. Y. & Wehrens, X. H. T. Emerging roles of junctophilin-2 in the heart and implications for cardiac diseases. *Cardiovascular Research* **103**, 198–205 (2014).

47. Marston, S. Obscurin variants and inherited cardiomyopathies. *Biophys Rev* **9**, 239–243 (2017).

48. Marian, A. j. Molecular Genetic Basis of Hypertrophic Cardiomyopathy. *Circulation Research* **128**, 1533–1553 (2021).

49. Coats, C. J. *et al.* Proteomic Analysis of the Myocardium in Hypertrophic Obstructive Cardiomyopathy. *Circulation: Genomic and Precision Medicine* **11**, e001974 (2018).

50. Gilda, J. E., Lai, X., Witzmann, F. A. & Gomes, A. V. Delineation of Molecular Pathways Involved in Cardiomyopathies Caused by Troponin T Mutations. *Molecular & Cellular Proteomics* **15**, 1962–1981 (2016).

51. Shao, D. & Tian, R. Glucose Transporters in Cardiac Metabolism and Hypertrophy. *Compr Physiol* **6**, 331–351 (2015).

52. Razeghi, P. *et al.* Metabolic gene expression in fetal and failing human heart. *Circulation* **104**, 2923–2931 (2001).

53. Pound, K. M. *et al.* Expression of slow skeletal TnI in adult mouse hearts confers metabolic protection to ischemia. *Journal of Molecular and Cellular Cardiology* **51**, 236–243 (2011).

54. Vakrou, S. & Abraham, M. R. Hypertrophic cardiomyopathy: a heart in need of an energy bar? *Frontiers in Physiology* **5**, (2014).

55. Ranjbarvaziri, S. *et al.* Altered Cardiac Energetics and Mitochondrial Dysfunction in Hypertrophic Cardiomyopathy. *Circulation* **144**, 1714–1731 (2021).

56. Schmid, M. & Toepfer, C. N. Cardiac myosin super relaxation (SRX): a perspective on fundamental biology, human disease and therapeutics. *Biology Open* **10**, bio057646 (2021).

57. Sadayappan, S. *et al.* Cardiac Myosin-Binding Protein-C Phosphorylation and Cardiac Function. *Circulation Research* **97**, 1156–1163 (2005).

58. Rosas, P. C. & Solaro, R. J. Implications of S-glutathionylation of sarcomere proteins in cardiac disorders, therapies, and diagnosis. *Frontiers in Cardiovascular Medicine* **9**, (2023).

59. Kaski, J. P. *et al.* Outcomes after implantable cardioverter-defibrillator treatment in children with hypertrophic cardiomyopathy. *Heart* **93**, 372–374 (2007).

60. Van Driest, S. L. *et al.* Prevalence and spectrum of thin filament mutations in an outpatient referral population with hypertrophic cardiomyopathy. *Circulation* **108**, 445–451 (2003).

61. Watkins, H. *et al.* Mutations in the genes for cardiac troponin T and alpha-tropomyosin in hypertrophic cardiomyopathy. *N Engl J Med* **332**, 1058–1064 (1995).

62. Gomes, A. V., Guzman, G., Zhao, J. & Potter, J. D. Cardiac troponin T isoforms affect the Ca2+ sensitivity and inhibition of force development. Insights into the role of troponin T isoforms in the heart. *J Biol Chem* **277**, 35341–35349 (2002).

63. Miller, T. *et al.* Abnormal contractile function in transgenic mice expressing a familial hypertrophic cardiomyopathy-linked troponin T (I79N) mutation. *J Biol Chem* **276**, 3743–3755 (2001).

64. Bers, D. M. Calcium fluxes involved in control of cardiac myocyte contraction. *Circ Res* **87**, 275–281 (2000).

65. Qu, Z., Liu, M. B. & Nivala, M. A unified theory of calcium alternans in ventricular myocytes. *Sci Rep* **6**, 35625 (2016).

66. Rovetti, R., Cui, X., Garfinkel, A., Weiss, J. N. & Qu, Z. Spark-Induced Sparks as a Mechanism of Intracellular Calcium Alternans in Cardiac Myocytes. *Circulation Research* **106**, 1582–1591 (2010).

67. Nivala, M., de Lange, E., Rovetti, R. & Qu, Z. Computational Modeling and Numerical Methods for Spatiotemporal Calcium Cycling in Ventricular Myocytes. *Frontiers in Physiology* **3**, (2012).

Figure 1. Computational modelling and potential energy minimization. **Panels A. and B.** show troponin T (cyan), actin chain F (brown), tropomyosin chain W (green), and tropomyosin chain X (purple). **Panel A.** shows the structure of the complex with WT troponin T (with residue R278). **Panel B.** includes the predicted structure of the complex with the genetic variant *TNNT2* R278C$^{+/-}$. Residues with side chain atoms displayed correspond to the five closest residues that the R278 CG (γ carbon) atom and C278 SG (γ sulfur) atom have in common. **Panels C. and D.** show troponin T (cyan) and the surfaces of actin chain F and tropomyosin chain W. The surfaces of these chains are colored with respect to their Coulombic surface potential, where blue indicates positive residues, red indicates negative residues, and white corresponds to neutral residues. **Panel C.** shows the structure of the complex with R278, and **Panel D.** shows the modelled structure of the Tn complex that harbors the mutant residue C278. Labels shown are in the format: one letter residue code, residue number, chain ID.

Figure 2. Steady-state and stopped-flow analysis of Ca^{2+} kinetics in human cardiac reconstituted thin filaments (hcRTF). Panel A. The Ca^{2+} sensitivity (expressed in K_d (μM)) of the WT and R278C$^{+/-}$ hcRTF was determined by steady-state fluorescence spectrometry. The R278C significantly decreased the K_d compared to the WT counterpart by ~2-fold, indicating that this variant increases the Ca^{2+} sensitivity significantly in the hcRTF biochemical system. Panel B. A stopped-flow instrument was used to determine the Ca^{2+} dissociation rates (expressed in k_{off} (s^{-1})) from the hcRTF. Upon the addition of EGTA, the Ca^{2+} was rapidly removed from TnC, inducing a conformational change in cTnC within hcRTF in which the fluorescence change was recorded. The R278C$^{+/-}$ hcRTF exhibited a decrease in the k_{off} by ~1.5 fold, compared to the WT counterpart, suggesting that the increase in Ca^{2+} sensitivity observed in the steady state is largely due to a slower Ca^{2+} off-loading rate. *p<0.05, **p<0.05, ***p<0.005.

Figure 3. MS proteomic abundance profiles. Panel A. Volcano plot comparison of WT vs. R278C$^{+/-}$ on the protein expression levels. The right side of the plot (red) reflects upregulated proteins in R278C$^{+/-}$ hiPSC-CMs, and the left side (black) shows the proteins that were detected in higher quantity in the WT hiPSC-CMs. The FDR threshold was set to 0.01, and any data points beyond that were considered as statistically significant. Gene ontology (GO) annotation terms summarize the top cross search results in reference to KEGG, Elsevier, Jensen, and GO biological processes databases. Panels B-D. Violin plot representations of individual proteins that exhibited significant changes between the R278C$^{+/-}$ vs. WT and separated according to their functional groups. Panel B. Thick filament proteins: MYH7 (myosin heavy chain-7), MYH6 (myosin heavy chain-6), MYL2 (myosin regulatory light chain ventricular isoform), and MYL6 (myosin regulatory light chain-6). Panel C. Z-disc proteins: ACTN1 (Alpha actinin-1), MYOZ2 (Myozenin-2), NEBL (Nebulette), PDLIM5 (PDZ and LIM domain protein-5), SMPX (Small muscular protein), and CSRP3 (Cysteine and glycine-rich protein-3). Panel D. Cardiac remodelling proteins: DESM (Desmin), JPH2 (Junctophilin-2), IQGAP1 (Ras GTPase-activating-like protein), OBSCN (Obscurin), FHL1 (Four and a half LIM domains protein-1), and FHL2 (Four and a half LIM domains protein-2). *p<0.05, **p<0.05, ***p<0.005; two-tailed unpaired t-test.

Figure 4. MS proteomic abundance profile of metabolic and energy production proteins. Panel A. PGAM1 (Phosphoglycerate mutase-1), PFKAM (ATP-dependent 6- phosphofructokinase, muscle type), GLUT1 (Solute carrier family 2, facilitated glucose transporter member-1). Panel B. ACADM (Medium-chain specific acyl-CoA dehydrogenase), ACADS (Short-chain specific acyl-CoA dehydrogenase), FABPH (Fatty acid binding protein, heart). Panel C. CKM (Creatine kinase M-type), CKMT2 (Creatine kinase mitochondrial type 2), and ATPD (ATP synthase subunit delta, mitochondrial). (* p-value< 0.05, ** p-value <0.005, ***p-value<0.0005; two-tailed unpaired t-test.)

Figure 5. Phosphorylation profile of six selected phosphosites in R278C$^{+/-}$ vs. WT hiPSC-CMs. Dot plot representation of the phosphorylation change relative to the total protein expression. The degree of WT phosphorylation was used as the baseline to compare the phosphorylation trends in the chosen phosphosites in the R278C$^{+/-}$ hiPSC-CMs.

Figure 6. Optical mapping (OM) of membrane voltage (V_m) and calcium (Ca^{2+}) transients in 2D monolayers of hiPSC-CMs. Panel A. Representative OM traces of V_m (red) and Ca^{2+} (black) transients in WT (A1 to A3) and R278C$^{+/-}$ (A4 to A6) hiPSC-CMs at three different stimulation frequencies 55, 65, 100 bpm in the top, middle, and bottom traces, respectively. WT hiPSCs responded normally to all stimulation frequencies, however, about 50% of R278C$^{+/-}$ hiPSC-CMs exhibited voltage and Ca^{2+} alternans at frequencies above 75 bpm. Panel B. Statistical analysis of action potential duration of WT (black) and R278C$^{+/-}$ (red) hiPSC-CMs as a function of stimulation frequencies over the range of 55 to 75 BPM. Panels B1 and B2 show that both the APD_{30} and APD_{80} were significantly longer in R278C$^{+/-}$ vs. WT at all stimulation frequencies. Panel C1 shows that the $CaTD_{30}$ was significantly longer in R278C$^{+/-}$ vs. WT at all stimulation frequencies. Panel C2 exhibits the longer $CaTD_{80}$ in R278C$^{+/-}$ vs WT hiPSCs at 65 and 75 bpm. (* p-value< 0.05, ** p-value <0.005, ***p-value<0.0005)

Figure 7. SarcTrack analysis of WT and R278C$^{+/-}$ hiPSC-CM contractile properties. Panel A. GFP-tagged α-actinin hiPSC-CMs cultured on 5 kPa PDMS (left) and SarcTrack wavelet fitting (right). Panel B. The relaxation of WT (black, n=9) and R278C$^{+/-}$ (red, n=12) hiPSC-CMs cultured on 5 kPa PDMS, with respect to: B1) time-to-half maximal relaxation (ms). B2) the maximum velocity of relaxation (µm. s-1). Panel C. The contractile parameters of WT (black, n=9) and R278C$^{+/-}$ (red, n=12) hiPSC-CMs cultured on 5 kPa PDMS and stimulated at 1 Hz with respect to: C1) percent maximal shortening; C2) time to half maximal contraction; C3) maximum velocity of contraction (µm s^{-1}). (* p-value< 0.05, ** p-value <0.005, ***p-value<0.0005)

Figure 8. SarcTrack analysis of the effect of mavacamten on R278C$^{+/-}$ hiPSC-CM contractile properties. Panel A. The effect of mavacamten on the contractile parameters of R278C$^{+/-}$ (red, n=37) hiPSC-CMs cultured on 5 kPa PDMS and stimulated at 1 Hz with respect to: A1) maximum velocity of contraction (µm. s^{-1}) and A2) percent maximal shortening. Panel B. The effect of Mavacamten on the relaxation of R278C$^{+/-}$ (red, n=37) hiPSC-CMs cultured on 5 kPa PDMS, with respect to the maximum velocity of relaxation (µm. s^{-1}). (* p-value< 0.05, ** p-value <0.005, ***p-value<0.0005)

Figure S1. Phylogenetic sequence alignment of cardiac troponin T (*TNNT2*). A multiple species sequence alignment of the cTnT protein (encoded by *TNNT2*) from human (Uniprot ID: P45379), bovine (Uniprot ID: P13789), rabbit (Uniprot ID: P09741), rat (Uniprot ID: P50753), mouse (Uniprot ID: P50752), chicken (Uniprot ID: P02642), and zebrafish (Uniprot ID: Q90Y46) was performed using Clustal Omega (Sievers et al., 2011). The equivalent residue R278 among all species are boxed in red and is shown to be highly conserved.

Figure S2. Genome Editing to Generate *TNNT2* R278C$^{+/-}$ and WT hiPSC-CMs. Panel A. Schematic of CRISPR/Cas9 design strategies to target R278 in *TNNT2* (R288 prior to postnatal Exon 5 alternative splicing) in two different hiPSC lines iPS(IMR900)-4 (sgRNA 1, ssODN 1, teal) and AICS-0075 cl.87 (sgRNA 2, ssODN 2, orange). The sequence shows the C>T mutation locus for R278C (highlighted in yellow). Panel B. Representative chromatograms of exon 16 in *TNNT2* from isolated iPS(IMR900)-4 (top) and AICS-0075 cl.87 (bottom) lines showing the heterozygous C>T base pair change as double-peaks post-editing for R278C. The C>A silent PAM site mutation is also shown in Design 2. The figure was created using Benchling and SnapGene software. WT = wild-type; hiPSC = human induced pluripotent stem cells; sgRNA = single guide RNA; ssODN = single-stranded oligonucleotide.

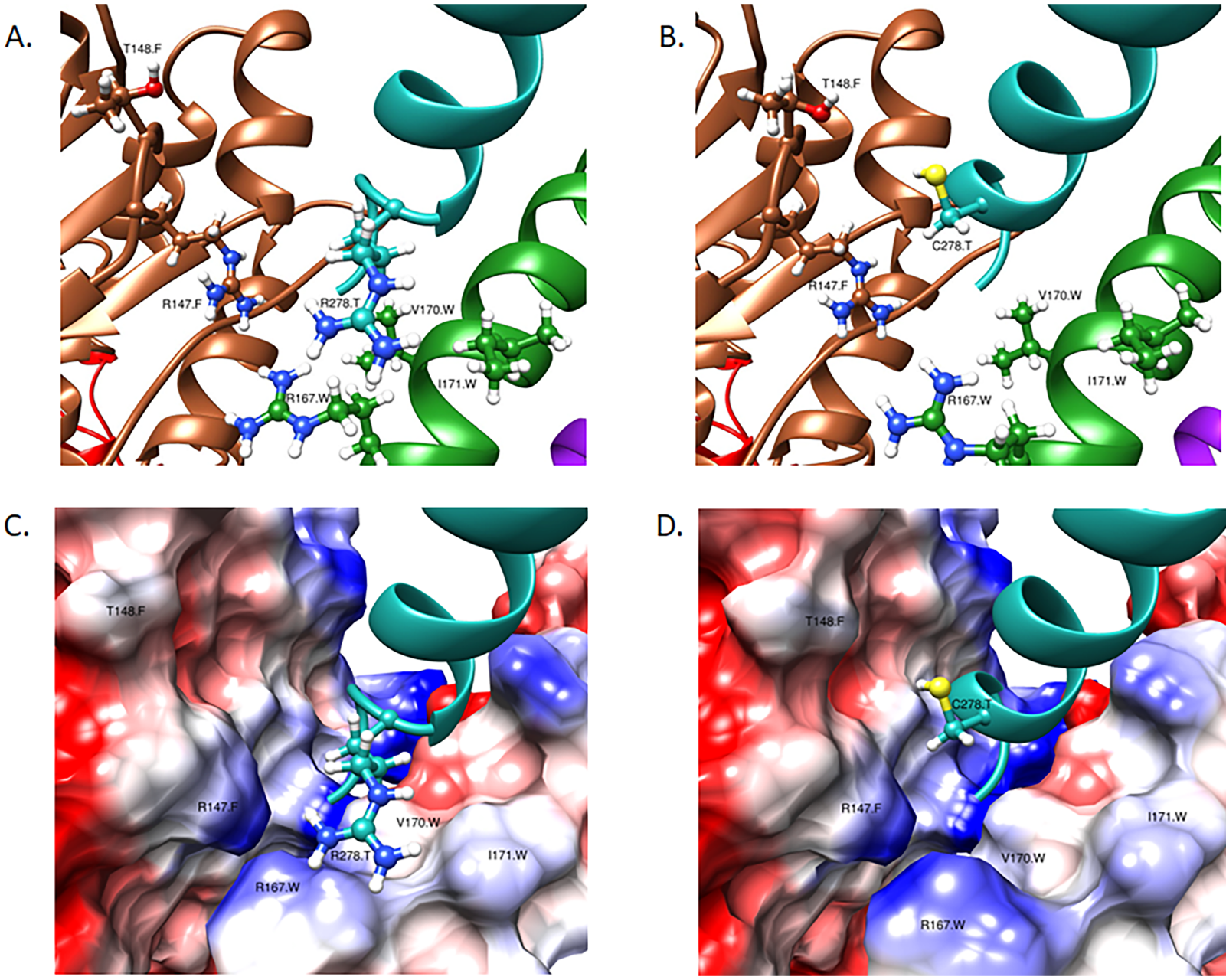
A.
T148.F
R147.F
R278.T
V170.W
I171.W
R167.W
B.
T148.F
C278.T
R147.F
V170.W
I171.W
R167.W
C.
T148.F
R147.F
V170.W
R278.T
I171.W
R167.W
D.
T148.F
C278.T
R147.F
I171.W
V170.W
R167.W

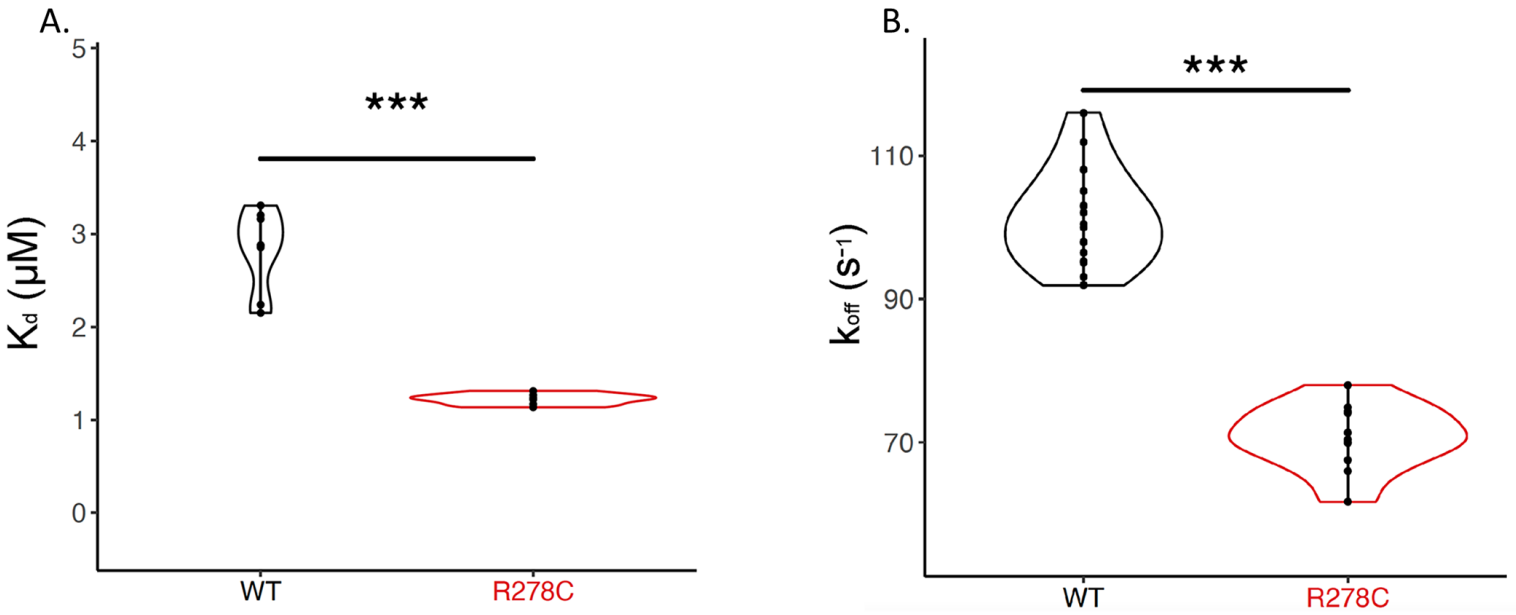
A.
***
K_d (μM)
5
4
3
2
1
0
WT
R278C
B.
***
k_{off} (s^{-1})
110
90
70
WT
R278C

Figure 3

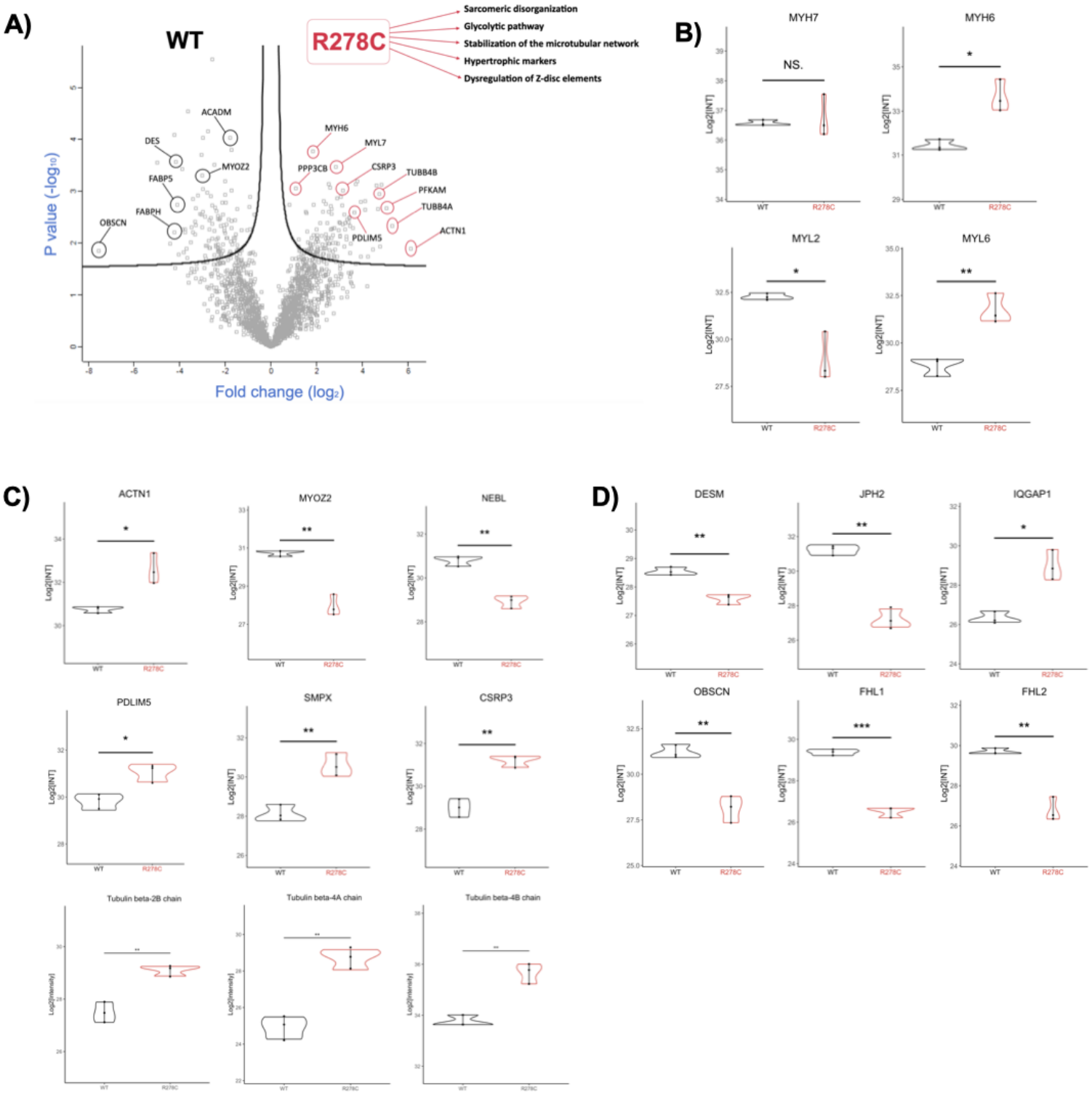
A)
WT
R278C
Sarcomeric disorganization
Glycolytic pathway
Stabilization of the microtubular network
Hypertrophic markers
Dysregulation of Z-disc elements
ACADM
DES
MYOZ2
FABP5
FABPH
OBSCN
MYH6
MYL7
PPP3CB
CSRP3
TUBB4B
PFKAM
TUBB4A
PDLIM5
ACTN1
P value (-log10)
Fold change (log2)
B)
MYH7
NS.
MYH6
MYL2
MYL6
Log2[INT]
WT
R278C
C)
ACTN1
MYOZ2
NEBL
PDLIM5
SMPX
CSRP3
Tubulin beta-2B chain
Tubulin beta-4A chain
Tubulin beta-4B chain
D)
DESM
JPH2
IQGAP1
OBSCN
FHL1
FHL2

Figure 4

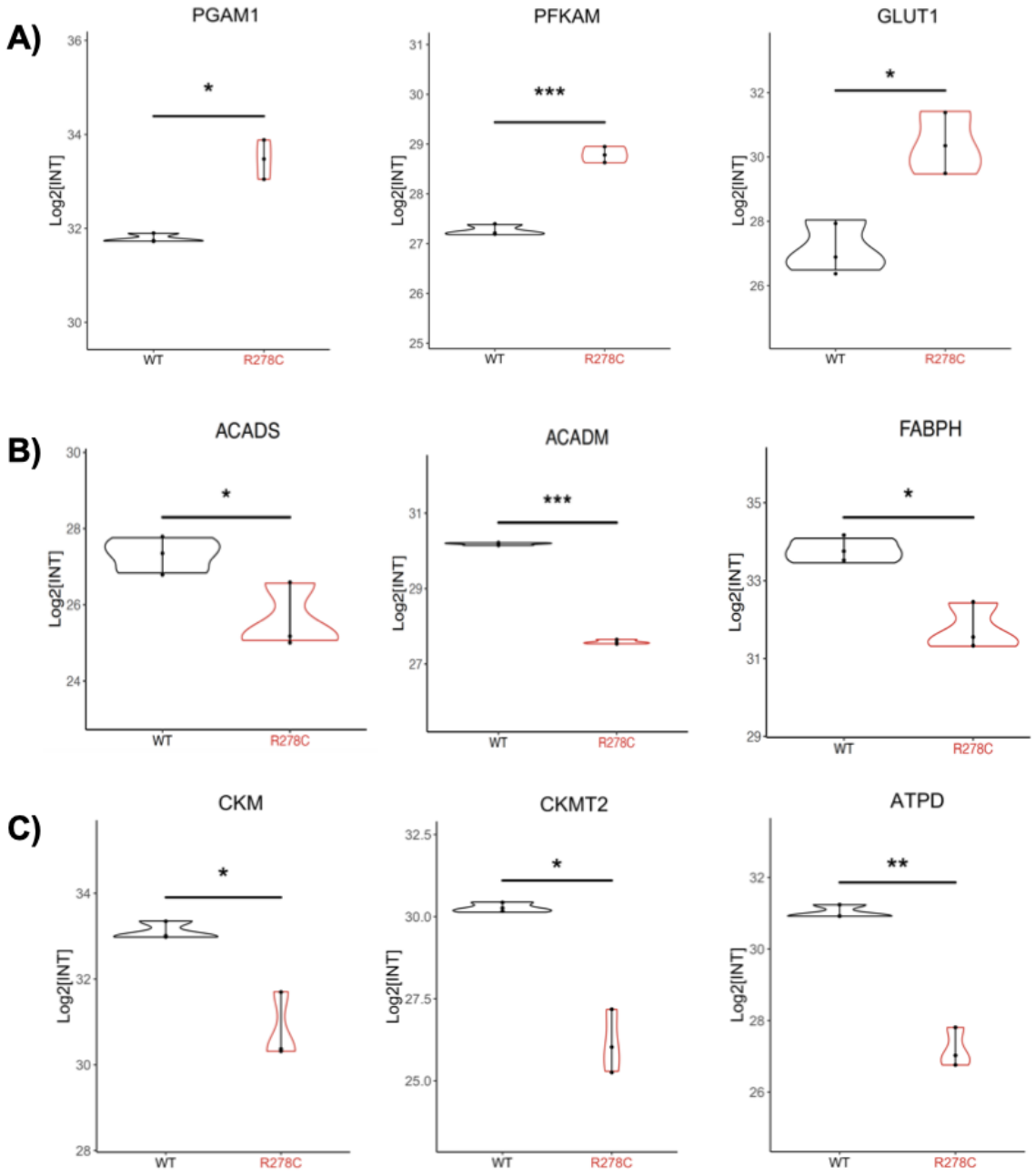
A)
PGAM1
PFKAM
GLUT1
B)
ACADS
ACADM
FABPH
C)
CKM
CKMT2
ATPD
Log2[INT]
WT
R278C
*
**
***

Figure 5

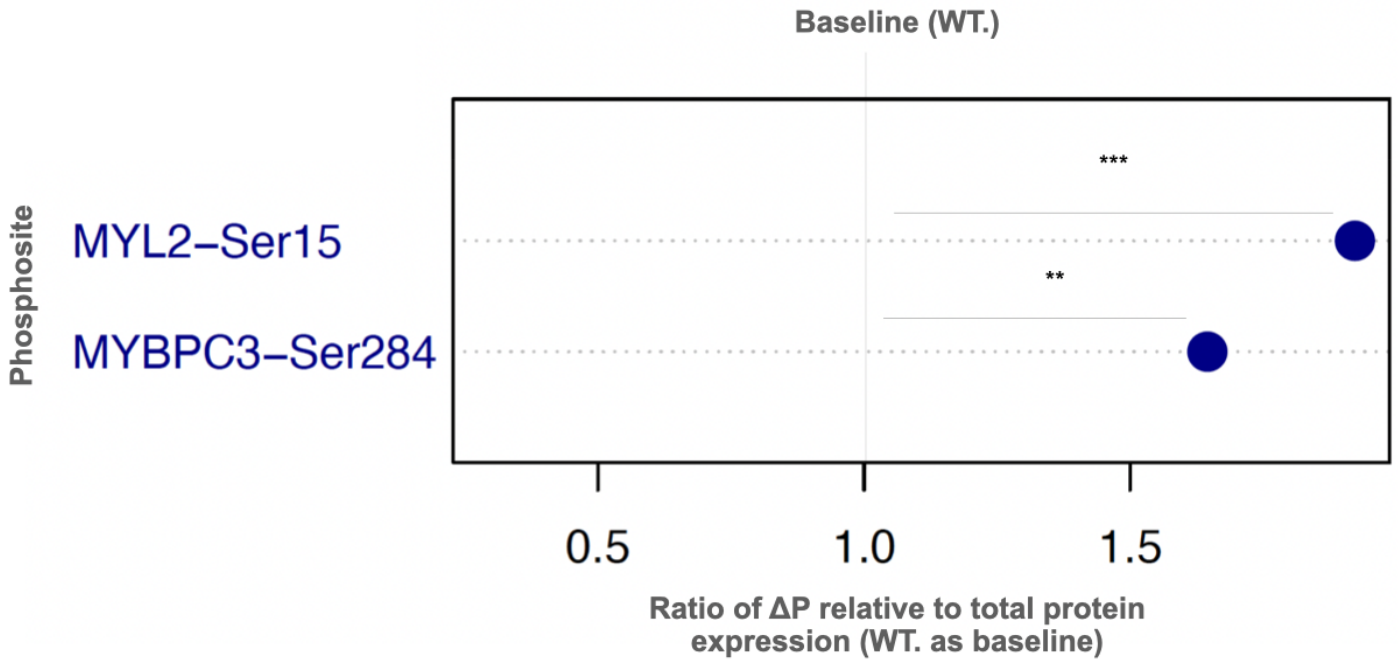
Baseline (WT.)
***
**
Phosphosite
MYL2–Ser15
MYBPC3–Ser284
0.5
1.0
1.5
Ratio of ΔP relative to total protein expression (WT. as baseline)

A. Representative voltage and Ca^{2+} transients

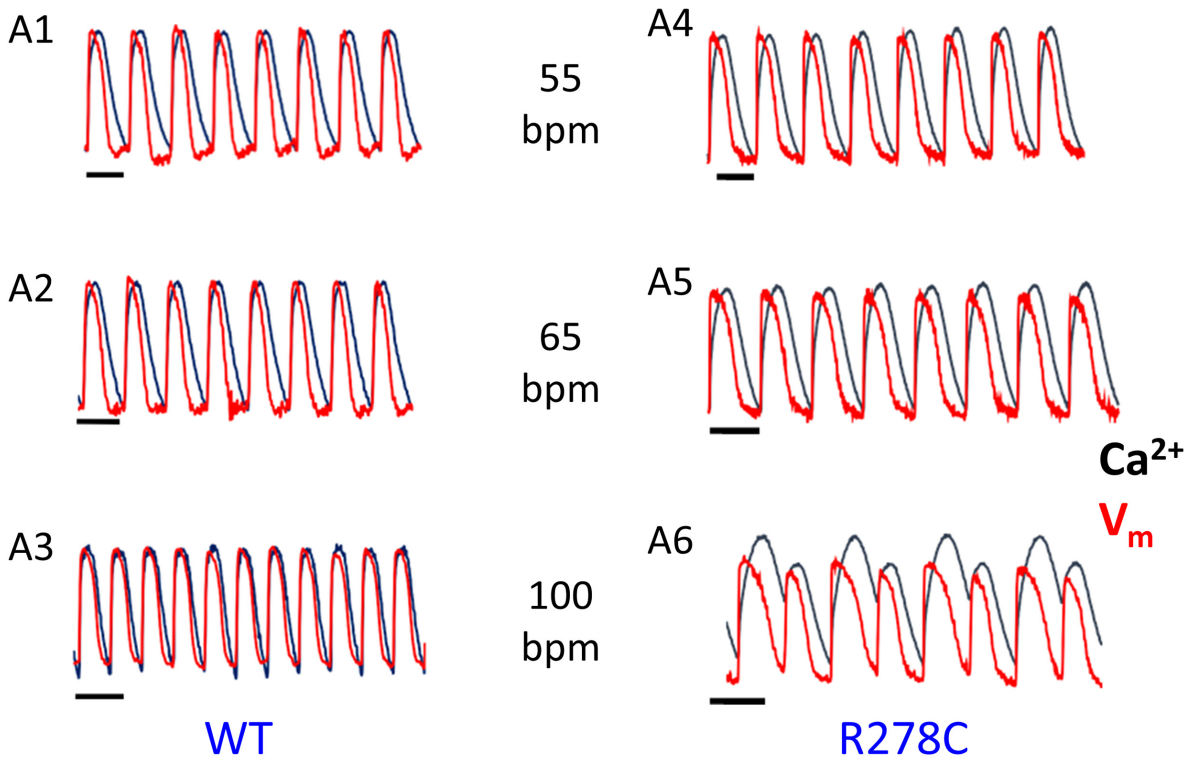

B. Action potential duration

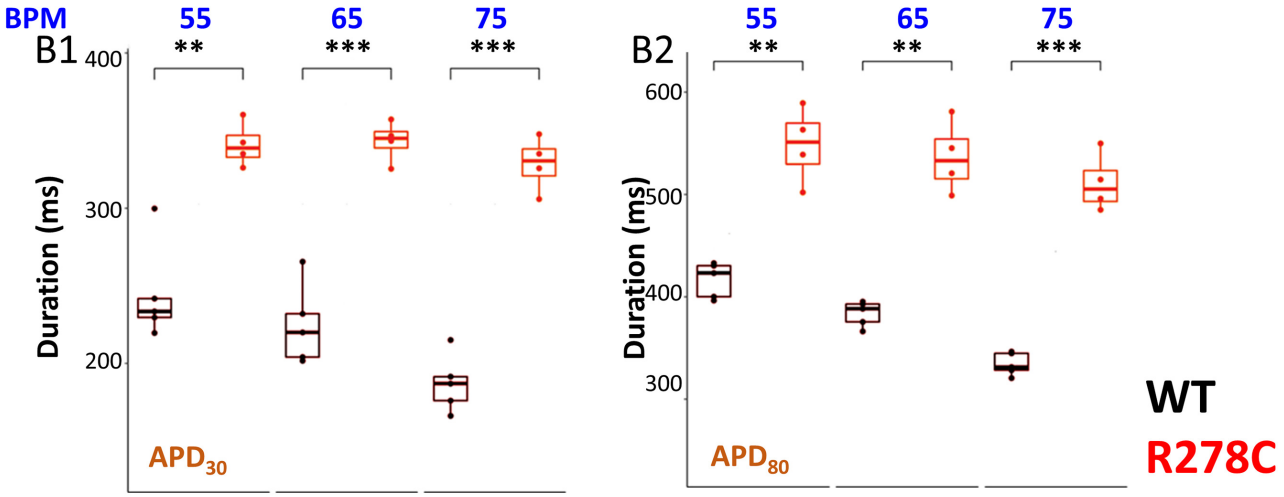

C. Ca^{2+} transient duration

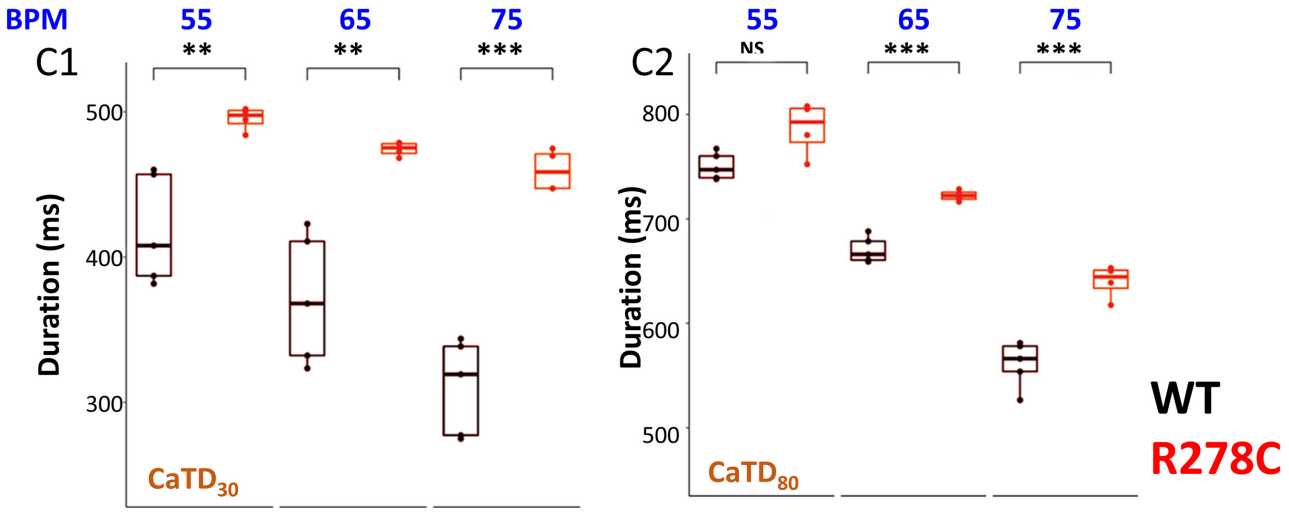

7A.

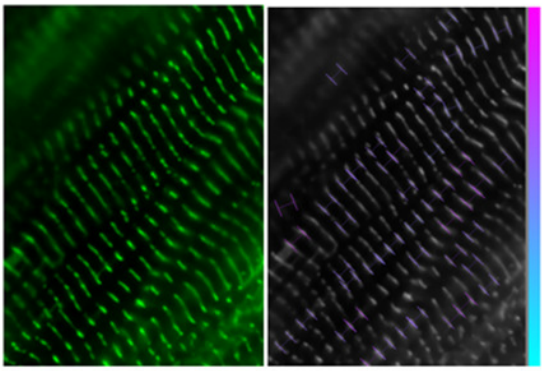

7B1.

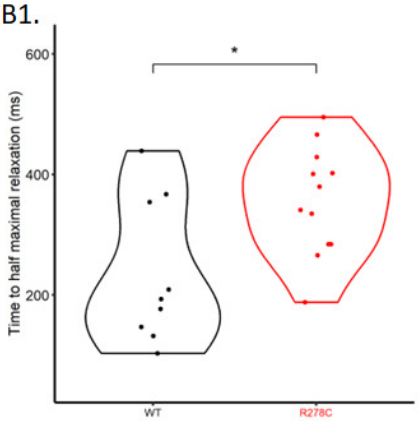

7B2.

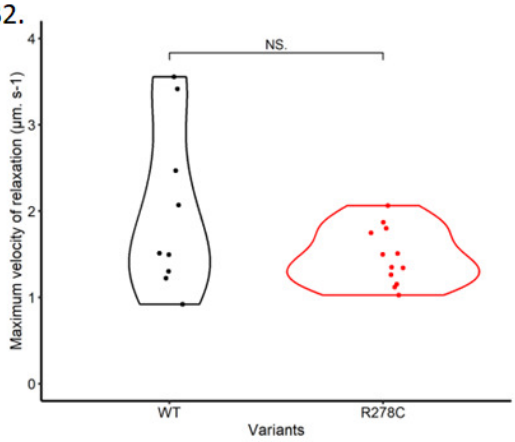

7C1.

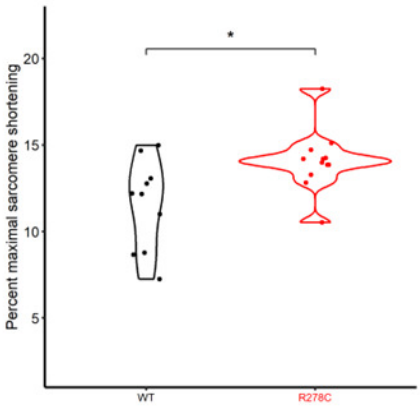

7C2.

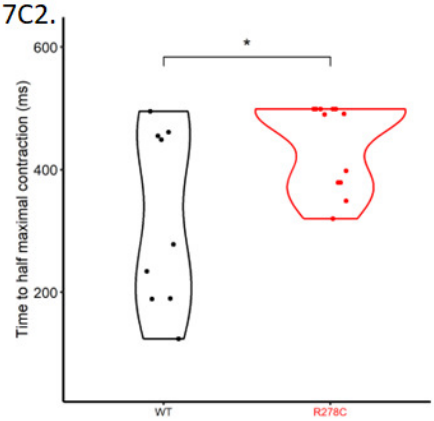

7C3.

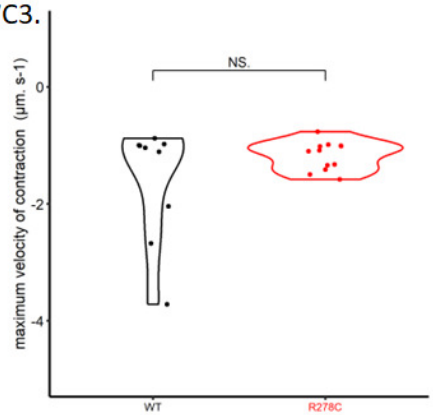

8A1.

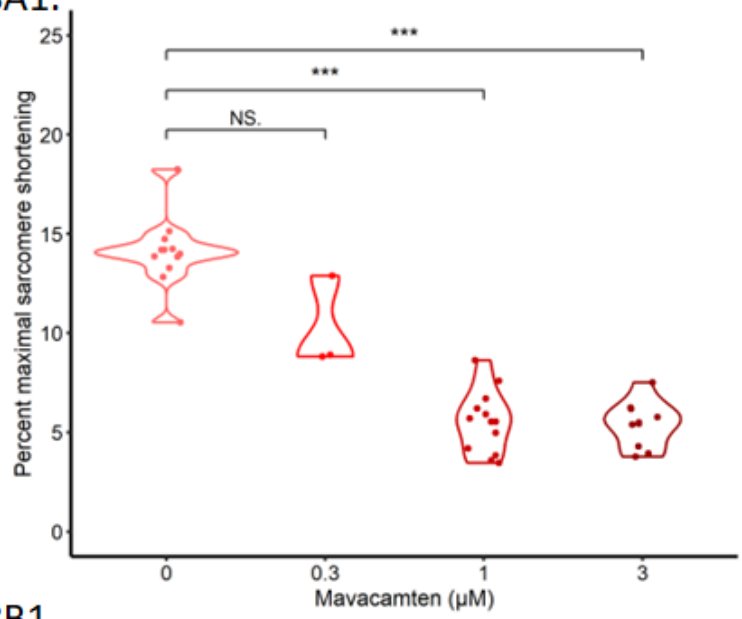
***
***
NS.
Percent maximal sarcomere shortening
25
20
15
10
5
0
0
0.3
1
3
Mavacamten (μM)

8A2.

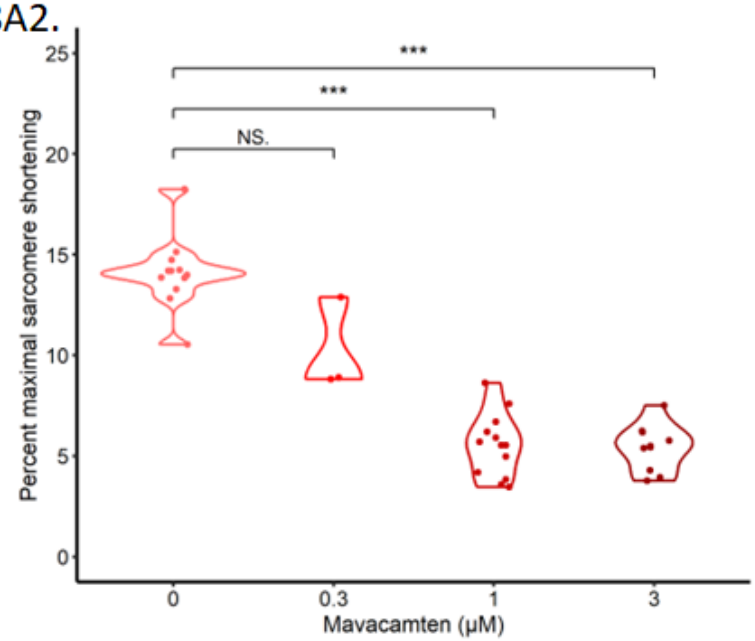
***
***
NS.
Percent maximal sarcomere shortening
25
20
15
10
5
0
0
0.3
1
3
Mavacamten (μM)

8B1.

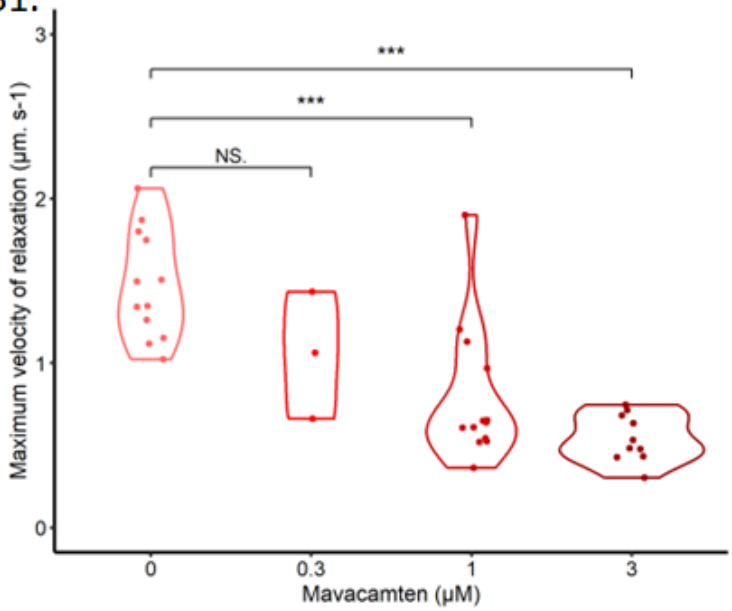
***
***
NS.
Maximum velocity of relaxation (μm. s-1)
3
2
1
0
0
0.3
1
3
Mavacamten (μM)

```
Human        AIDHLNEDQLREKAKELWQSIYNLEAEKFDLQEKFKQQKYEINVLRNRINDNQKVSK---    286
Bovine       AIDHLNEDQLREKAKELWQMIYDLEAEKFDLQEKFKQQKYEINVLRNRINDNQKVSK---    273
Rabbit       AIDHLNEDQLREKAKELWQSIYNLEAEKFDLQEKFKQQKYEINVLRNRINDNQKVSK---    289
Rat          AIDHLNEDQLREKAKELWQSIHNLEAEKFDLQEKFKQQKYEINVLRNRINDNQKVSK---    287
Mouse        AIDHLNEDQLREKAKELWQSIHNLEAEKFDLQEKFKQQKYEINVLRNRINDNQKVSK---    289
chicken      NIDHLSEDKLRDKAKELWQTIRDLEAEKFDLQEKFKRQKYEINVLRNRVSDHQKVKGSKA    290
Zebrafish    DIDNANESALREKAKELWSWMRELEAEKFELQYQFGKQKYEINVLRNRVSDHQKTSKRTK    277
              **: .*. **:******. : :******:** :* :***********:.*:**.

             R278
Human        TRGKAKVTGRWK 298
Bovine       TRGKAKVTGRWK 285
Rabbit       TRGKAKVTGRWK 301
Rat          TRGKAKVTGRWK 299
Mouse        TRGKAKVTGRWK 301
chicken      ARGKTMVGGRWK 302
Zebrafish    -RGLRK------ 282
              **
```

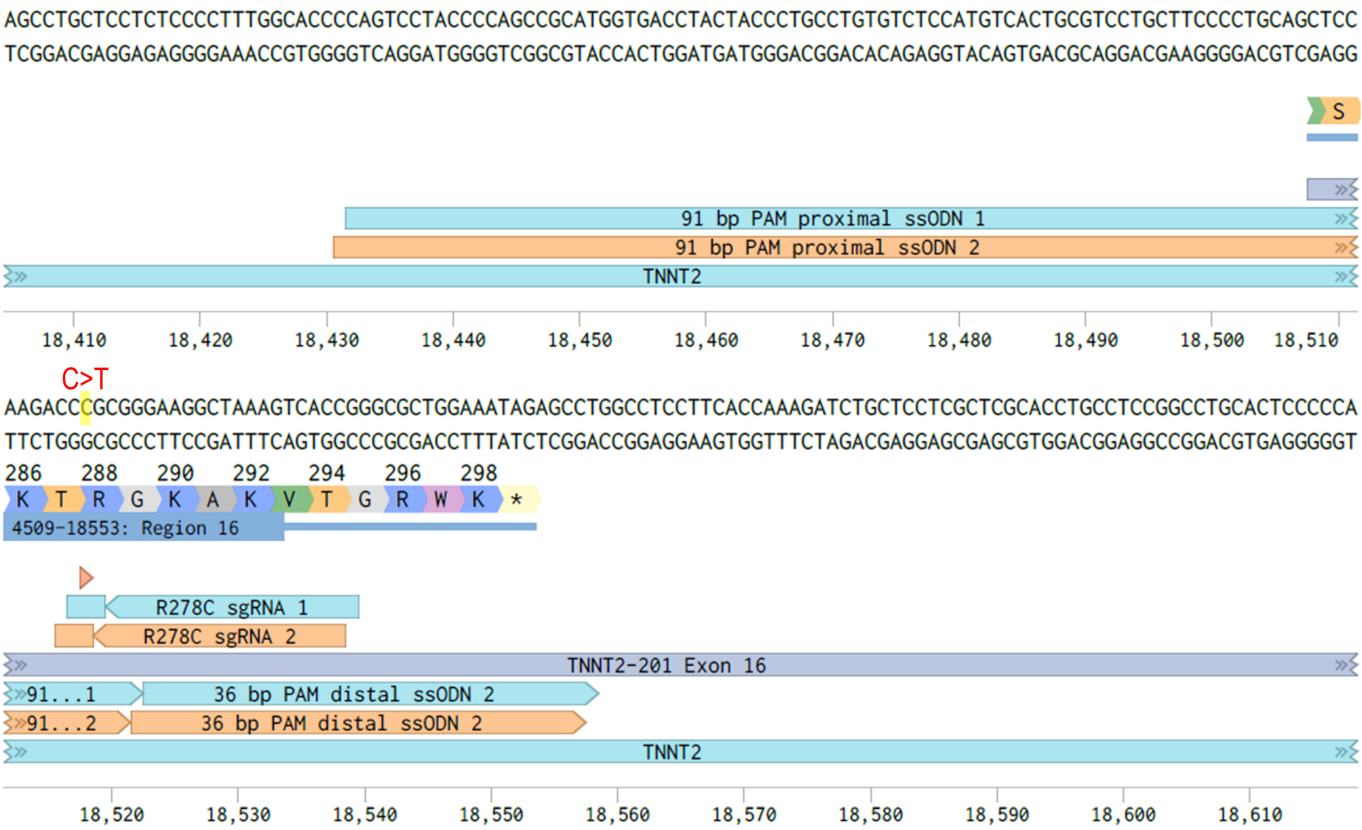

Design 1
iPS(IMR90)-4
R278C *TNNT2*

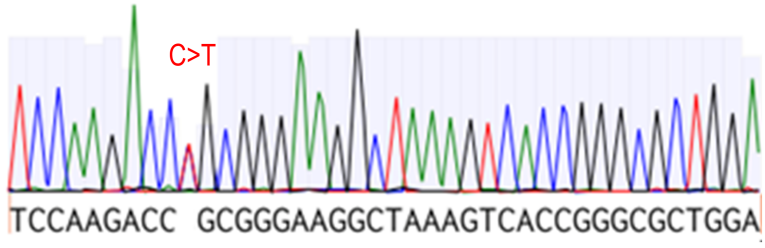
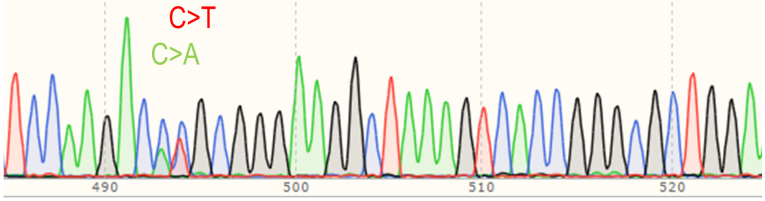
Design 2
AICS-0075 cl.87
R278C *TNNT2*